Inorganic Chemistry

Article

pubs.acs.org/IC

Theoretical Study of Mononuclear Nickel(I), Nickel(0), Copper(I), and Cobalt(I) Dioxygen Complexes: New Insight into Differences and Similarities in Geometry and Bonding Nature

Yue Chen and Shigeyoshi Sakaki*

Fukui Institute for Fundamental Chemistry, Kyoto University, Takano-Nishihiraki-cho 34-4, Sakyo-ku, Kyoto 606-8103, Japan

Supporting Information

ABSTRACT: Geometries, bonding nature, and electronic structures of (N^N)Ni(O_2) (N^N = β-diketiminate), its cobalt(I) and copper(I) analogues, and $(Ph_3P)_2Ni(O_2)$ were investigated by density functional theory (DFT) and multistate restricted active space multiconfigurational second-order perturbation (MS-RASPT2) methods. Only (N^N)Ni(O_2) takes a C_S symmetry structure, because of the pseudo-Jahn–Teller effect, while all other complexes take a C_{2V} structure. The symmetry lowering in (N^N)Ni(O_2) is induced by the presence of the singly occupied $\delta_{d_{xy}-\pi_x^*}$ orbital. In all of these complexes, significant superoxo (O_2^-) character is found from the occupation numbers of natural orbitals and the O–O π^* bond order, which is independent of the number of d electrons and the oxidation state of metal center. However, this is not a typical superoxo species, because the spin density is not found on the O_2 moiety, even in open-shell complexes, (N^N)Ni(O_2) and (N^N)Co(O_2). The M–O and O–O distances are considerably different from each other, despite the similar superoxo character. The M–O distance and the interaction energy between the metal and O_2 moieties are determined by the d_{yz} orbital energy of the metal moiety taking the valence state. The binding energy of the O_2 moiety is understood in terms of the d_{yz} orbital energy in the valence state and the promotion energy of the metal moiety from the ground state to the valence state. Because of the participations of various charge transfer (CT) interactions between the metal and O_2 moieties, neither the d_{yz} orbital energy nor the electron population of the O_2 moiety are clearly related to the O–O bond length. Here, the π bond order of the O_2 moiety is proposed as a good measure for discussing the O–O bond length. Because the d electron configuration is different among these complexes, the CT interactions are different, leading to the differences in the π bond order and, hence, the O–O distance among these complexes. The reactivity of dioxygen complex is discussed with the d_{yz} orbital energy.

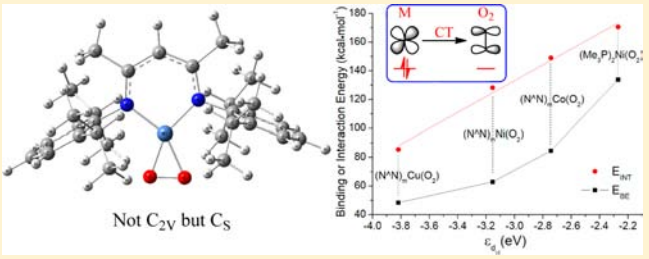

INTRODUCTION

Activation of dioxygen by such first-row transition metals as Mn, Fe, Co, Ni, and Cu plays crucial roles in biological oxidation.[1−6] For instance, the importance of copper dioxygen complex is well-recognized in bioinorganic chemistry.[7−13] In this regard, many efforts have been made to characterize the geometry, the electronic structure, the physicochemical property, and the nature of metal–dioxygen interaction of those dioxygen complexes.[7,14−23] However, the nickel–dioxygen interaction and the role of the Ni center in the relevant dioxygen complexes have been much less investigated than those of copper–dioxygen complexes,[3,24] despite the importance of the nickel–dioxygen species in superoxide dismutase.[25−27] It is of considerable importance to know how much and why the electronic structure and bonding interaction of the nickel dioxygen complex are different from and/or similar to those of the copper dioxygen complex. Such knowledge is indispensable for understanding the various metal dioxygen complexes in biological systems.

The first step of such research is to make comparison between mononuclear nickel–dioxygen complex and its copper analogue, because the mononuclear complex is simpler than the dinuclear complex. Also, the comparison of dinuclear metal–dioxygen complexes is not easily made because dinuclear copper–dioxygen complexes have been reported but a dinuclear nickel–dioxygen complex has not. On the other hand, the comparison can be easily made in mononuclear metal dioxygen complex, because the similar mononuclear dioxygen complexes have been reported in both nickel and copper cases. For instance, a nickel(0)–dioxygen complex $(Ph_3P)_2Ni(O_2)$ with a η^2 side-on coordination form was very previously reported.[28,29] Recently, Driess et al. reported a η^2 side-on nickel(I) dioxygen complex (N^N)Ni(O_2) (N^N = β-diketiminate).[30] The similar η^2 side-on copper(I)–dioxygen complex (N^N)Cu(O_2) was also reported slightly earlier[31,32] (see their structures in Scheme 1).

In general, the η^2 side-on M-O_2 moiety can be classified as either a superoxo (O_2^-) species with only one-electron charge transfer (CT) from the M to the O_2 in a formal sense or a peroxo (O_2^{2-}) one with two-electron CT.[33,34] In general, the complex with a longer O–O bond (1.4–1.5 Å) and a smaller O–O

Received: August 9, 2013
Published: November 6, 2013

Scheme 1. Real and Model Complexes of (N^N)Ni(O_2) and (N^N)Cu(O_2)

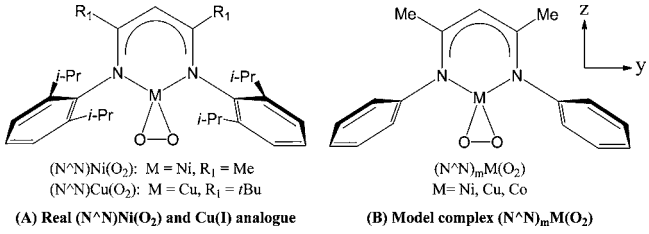

(N^N)Ni(O_2): M = Ni, R_1 = Me
(N^N)Cu(O_2): M = Cu, R_1 = *t*Bu

(A) Real (N^N)Ni(O_2) and Cu(I) analogue

$(N^N)_mM(O_2)$
M= Ni, Cu, Co

(B) Model complex $(N^N)_mM(O_2)$

stretching vibration (800−930 cm^{-1}) is understood as a peroxo form, while that with a shorter O−O bond length (1.2−1.3 Å) and a larger O−O vibration (1050−1200 cm^{-1}) is considered as a superoxo form.[14,19] Cramer et al. made successful comparisons among many transition-metal−dioxygen complexes and found that the O−O bond length and the stretching frequency correlate with the O−O bond order and those properties depend closely on the nature of the metal and its supporting ligands.[15,18,19] To date, the majority of the known η^2 side-on dioxygen complexes are described as a peroxo type.[14,35] In the η^2 side-on nickel(I)−dioxygen complex (N^N)Ni(O_2), the O−O bond length is 1.347 Å and the O−O stretching vibration is 971 cm^{-1} (see Scheme 1).[30] These data suggest that (N^N)Ni(O_2) is midway between the peroxo and the superoxo forms. The electron paramagnetic resonance (EPR) spectrum shows that this complex has a paramagnetic doublet ground state (total spin $\mathbf{S} = {}^1/_2$). DFT calculation with the B3LYP functional indicates that one unpaired electron is predominantly localized in the O_2 moiety; in other words, this is a superoxo complex.[30] Subsequently, Calzado and co-workers theoretically analyzed the electronic structure of this complex by a difference dedicated configuration interaction (DDCI) method and proposed that this complex exhibits a marked leading superoxo nature.[36] Calzado et al. also studied the copper(I) analogue (N^N)Cu(O_2) by the same method and proposed that (N^N)Cu(O_2) also is a superoxo complex.[36,37] However, this understanding is not consistent with the experimental and theoretical proposal that (N^N)Cu(O_2) has a singlet ground state with significant Cu(III)-peroxo character.[12,31,32,34,38−40] More importantly, (N^N)Ni(O_2) performed dioxygenase-like reactivity[41] but (N^N)Cu(O_2) is inert[15,42] in hydrogen abstraction from O−H and N−H groups. Both are different from the reactivity of typical superoxo species of cobalt,[43] iron,[44] and copper[45,46] dioxygen complexes. These reactivities are also related to their electronic structure and spin density.

Considering the above-mentioned confusing situation and novel reactivity of (N^N)Ni(O_2), it is interesting to investigate the differences and/or similarities among (N^N)Ni(O_2), (N^N)Cu(O_2), and $(Ph_3P)_2Ni(O_2)$. Such knowledge leads to a fundamental understanding of geometry, electronic structure, metal−dioxygen bonding nature, and their relations to the number of d electrons and the oxidation state in transition-metal dioxygen complexes.

In the present work, we theoretically investigated (N^N)Ni(O_2), its cobalt(I) and copper(I) analogues, and $(Ph_3P)_2Ni(O_2)$ by density functional theory (DFT) and multistate restricted active space multiconfigurational second-order perturbation (MS-RASPT2)[47] method with a large active space. We selected these complexes in expectation that we can clarify the differences and/or similarities among cobalt(I), nickel(I), and copper(I), and between nickel(I) and nickel(0). Our purposes here are:

(1) To elucidate the electronic structures of these complexes, in particular, to elucidate which understanding of peroxo and superoxo is correct in these complexes;
(2) To disclose the metal and ligand effects on the M−O_2 interaction;
(3) To find the determining factors for the M−O and the O−O bond lengths and their bonding natures, and
(4) The relation between reactivity of dioxygen complex and their electronic structure.

During this work, we found that pseudo-Jahn−Teller[48−50] distortion occurs only in (N^N)Ni(O_2): it is not observed in the other three complexes.

COMPUTATIONAL DETAILS AND MODEL

Because the transition-metal−dioxygen complex exhibits multiconfigurational character in many cases, we employed the MS-RASPT2 method here, including both static and dynamic electron correlation effects. Unfortunately, however, the geometry optimization by the MS-RASPT2 is considerably expensive, because of the lack of analytical gradient and the need of large memory space and disk space. Here, we employed the DFT method for geometry optimization with an appropriate DFT functional and analyzed the electronic structure by the MS-RASPT2 method with the DFT-optimized geometry. To select a suitable DFT functional, we optimized the geometry of (N^N)Ni(O_2) and compared it with the experimental one (see page S3 and Table S1 in the Supporting Information. After careful examinations, we selected the TPSSTPSS functional[51] in this work, because the TPSSTPSS-optimized geometry agrees well with the experimental one.

The active space of RASSCF calculation was selected as follows: In the O_2 moiety, the two π^* orbitals are important. In the N^N ligand, three π and two π^* orbitals exist around the HOMO and LUMO of (N^N)Ni(O_2). For the first-row transition metals, we need to consider the double-shell effect,[12,52,53] because of the strong correlation effect. As a result, a total of 17 electrons in 17 orbitals must be involved in the active space of CASSCF calculation of (N^N)Ni(O_2). However, such CASSCF calculation cannot be carried out, even nowadays. Thus, the entire active space is separated into RAS2 and RAS3 subspaces. In the RAS3 subspace, five 4d-like orbitals are included. Five 3d orbitals of metal, two π^* orbitals of the O_2 moiety, and three π and two π^* orbitals of the N^N ligand are included in the RAS2 space. In the RASSCF calculation, one-electron excitations from the RAS2 to the RAS3 are considered (see Figure S2 in the Supporting Information). This is not unreasonable, because the occupation numbers of the 4d orbitals are very small (see Table S2 in the Supporting Information). In (N^N)Cu(O_2) and (N^N)Co(O_2), 18 and 16 electrons are considered, respectively, with the same active orbitals as those of the Ni analogue.

For both DFT and MS-RASPT2 calculations, the same basis set system was used. The (311111/22111/411/1) basis sets were used for Ni, Cu, and Co and the effective core potentials proposed by the Stuggart−Dresden−Bonn group[54] were employed for transition metals. The cc-pVDZ basis sets were used for C, N, O, and H atoms, where one augmented function was added to each O atom. All the DFT calculations were carried out using the Gaussian 09 program package[55] and MS-RASPT2 calculations were performed using the MOLCAS 7.6 program package.[56−58]

Model complexes $(N^N)_mM(O_2)$ were employed to analyze the electronic stucture to save computer processing unit (CPU) time, in which the *i*-propyl substitutents on the N^N were substituted for H atoms, as shown in Scheme 1. [Note that the subscript "m" means the model hereafter.] We believe that this model is reasonable because the geometry and electronic structure of the M−O_2 moiety are essentially the same as those of the real complex, as will be discussed below.

The hydrogen abstraction reactions by these dioxygen complexes were investigated here. The geometry changes were optimized with the B3LYP functional, because the use of the B3LYP was recommended for the geometry optimization of the hydrogen-abstraction reaction.[59,60] The electronic energy was recalculated with the TPSSTPSS functional, which was also recommended previously for evaluating energy changes

dx.doi.org/10.1021/ic402059b | Inorg. Chem. 2013, 52, 13146−13159

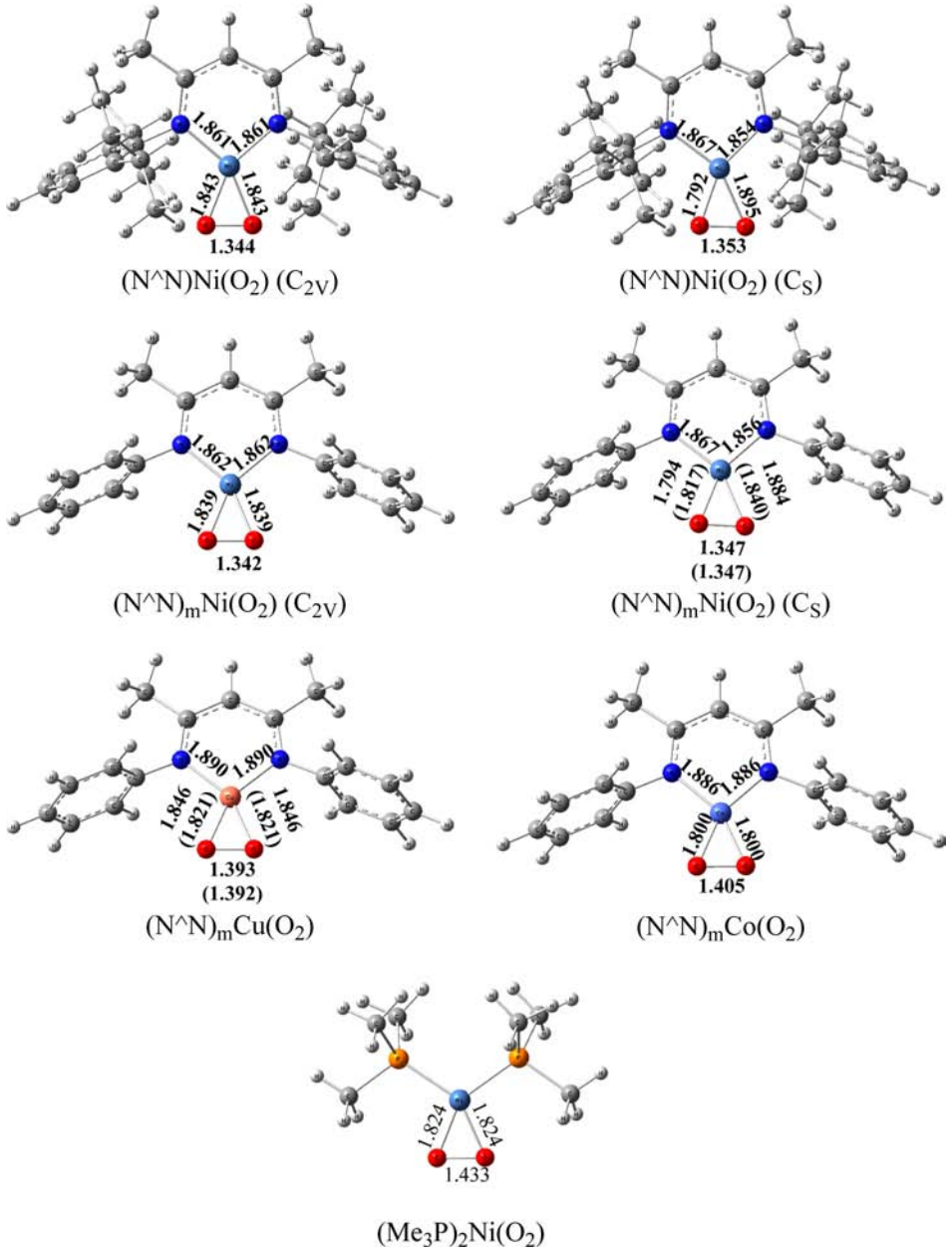

Figure 1. Optimized structures of $(N^{\wedge}N)Ni(O_2)$, $(N^{\wedge}N)_mM(O_2)$, and $(Me_3P)_2Ni(O_2)$. [In this figure, the DFT(TPSSTPSS) method was employed; the experimental values (given in Ångstroms) are shown in parentheses.]

of the hydrogen abstraction reaction.[60] For these calculations, model complex $(N^{\wedge}N)_mM(O_2)$ was employed, because it is likely to make comparison among the different metals with this model system. All the Gibbs energies were calculated at a temperature of 298.15 K in the gas phase, where the TPSSTPSS-calculated electronic energy and B3LYP-calculated enthalpy and entropy were employed (see Table S4 in the Supporting Information).

RESULTS AND DISCUSSION

Geometries of $(N^{\wedge}N)Ni(O_2)$, $(N^{\wedge}N)Cu(O_2)$, $(N^{\wedge}N)Co(O_2)$, and $(Ph_3P)_2Ni(O_2)$. The TPSSTPSS-optimized geometry of $(N^{\wedge}N)Ni(O_2)$ agrees well with the experimental one, as shown in Figure 1. However, the optimized C_{2V} symmetrical geometry exhibits a significantly large imaginary frequency ($459i$ cm^{-1}), which is the asymmetrical in-plane stretching of Ni−O bonds; see Page S3 and Table S1 in the Supporting Information for details. Hence, we reoptimized this complex under both C_S and C_1 symmetry. The C_S symmetry structure is similar to the C_1 symmetry one, and the difference in total energy between them is not very different; see pages S3−S4 in the Supporting Information for more details. The C_S-optimized geometry agrees well with the experimental one, too. It is slightly more stable than the C_{2V} one, where the energy difference is 0.2 kcal mol^{-1}. Because bulky substituents are introduced in the $N^{\wedge}N$ ligand, we investigated a model complex $(N^{\wedge}N)_mNi(O_2)$ (see Scheme 1) without bulky substituents to check the possibility that the steric effect of bulky substituents induces the symmetry lowering. The C_{2V} symmetry model complex $(N^{\wedge}N)_mNi(O_2)$ also exhibits an imaginary frequency ($357i$ cm^{-1}) like the real compound $(N^{\wedge}N)Ni(O_2)$. In $(N^{\wedge}N)_mNi(O_2)$, two Ni−O, two Ni−N, and O−O bond lengths are close to those of the experimental values of the real compound (Figure 1). It should be noted that the O−O bond length, which is an important geometrical parameter, is almost the same as the experimental one. The C_S symmetry

dx.doi.org/10.1021/ic402059b | Inorg. Chem. 2013, 52, 13146−13159

Table 1. Relative Energies of the Ground and Low-Lying Excited States of Model Complexes

state (symmetry)	configurations	weight (%)	relative energy (kcal mol^{-1})
	$(N^{\wedge}N)_mNi(O_2)$ (C_{2V})		
ground state ($^2A''$)	$\pi^{2}_{\pi_z^*+d_{yz}}\delta^{2}_{\pi_x^*+d_{xy}}d^{2}_{y^2-z^2}d^{2}_{x^2}d^{2}_{xz}\delta^{*1}_{d_{xy}-\pi_x^*}\pi^{*0}_{\pi_z^*-d_{yz}}$	61.4	0.0
	$\left(\pi^{0}_{\pi_z^*+d_{yz}}\delta^{2}_{\pi_x^*+d_{xy}}d^{2}_{y^2-z^2}d^{2}_{x^2}d^{2}_{xz}\delta^{*1}_{d_{xy}-\pi_x^*}\pi^{*2}_{\pi_z^*-d_{yz}}\right)$	6.2	
first excited state ($^2A''$)	$\pi^{2}_{\pi_z^*+d_{yz}}\delta^{2}_{\pi_x^*+d_{xy}}d^{2}_{y^2-z^2}d^{2}_{x^2}d^{1}_{xz}\delta^{*2}_{d_{xy}-\pi_x^*}\pi^{*0}_{\pi_z^*-d_{yz}}$	62.9	1.8
	$\left(\pi^{0}_{\pi_z^*+d_{yz}}\delta^{2}_{\pi_x^*+d_{xy}}d^{2}_{y^2-z^2}d^{2}_{x^2}d^{1}_{xz}\delta^{*2}_{d_{xy}-\pi_x^*}\pi^{*2}_{\pi_z^*-d_{yz}}\right)$	8.9	
second excited state ($^2A'$)	$\pi^{2}_{\pi_z^*+d_{yz}}\delta^{2}_{\pi_x^*+d_{xy}}d^{2}_{y^2-z^2}d^{1}_{x^2}d^{2}_{xz}\delta^{*2}_{d_{xy}-\pi_x^*}\pi^{*0}_{\pi_z^*-d_{yz}}$	57.5	2.9
	$\left(\pi^{1}_{\pi_z^*+d_{yz}}\delta^{2}_{\pi_x^*+d_{xy}}d^{2}_{y^2-z^2}d^{1}_{x^2}d^{2}_{xz}\delta^{*2}_{d_{xy}-\pi_x^*}\pi^{*1}_{\pi_z^*-d_{yz}}\right)$	10.8	
	$(N^{\wedge}N)_mNi(O_2)$ (C_S)		
ground state ($^2A''$)	$\pi^{2}_{\pi_z^*+d_{yz}}\delta^{2}_{\pi_x^*+d_{xy}}d^{2}_{y^2-z^2}d^{2}_{x^2}d^{2}_{xz}\delta^{*1}_{d_{xy}-\pi_x^*}\pi^{*0}_{\pi_z^*-d_{yz}}$	44.1	−1.0
	$\left(\pi^{2}_{\pi_z^*+d_{yz}}\delta^{2}_{\pi_x^*+d_{xy}}d^{2}_{y^2-z^2}d^{2}_{x^2}d^{1}_{xz}\delta^{*2}_{d_{xy}-\pi_x^*}\pi^{*0}_{\pi_z^*-d_{yz}}\right)$	17.6	
first excited state ($^2A''$)	$\pi^{2}_{\pi_z^*+d_{yz}}\delta^{2}_{\pi_x^*+d_{xy}}d^{2}_{y^2-z^2}d^{2}_{x^2}d^{1}_{xz}\delta^{*2}_{d_{xy}-\pi_x^*}\pi^{*0}_{\pi_z^*-d_{yz}}$	45.2	3.3
	$\left(\pi^{2}_{\pi_z^*+d_{yz}}\delta^{2}_{\pi_x^*+d_{xy}}d^{2}_{y^2-z^2}d^{2}_{x^2}d^{2}_{xz}\delta^{*1}_{d_{xy}-\pi_x^*}\pi^{*0}_{\pi_z^*-d_{yz}}\right)$	17.2	
second excited state ($^2A'$)	$\pi^{2}_{\pi_z^*+d_{yz}}\delta^{2}_{\pi_x^*+d_{xy}}d^{2}_{y^2-z^2}d^{1}_{x^2}d^{2}_{xz}\delta^{*2}_{d_{xy}-\pi_x^*}\pi^{*0}_{\pi_z^*-d_{yz}}$	55.8	5.1
	$\left(\pi^{1}_{\pi_z^*+d_{yz}}\delta^{2}_{\pi_x^*+d_{xy}}d^{2}_{y^2-z^2}d^{1}_{x^2}d^{2}_{xz}\delta^{*2}_{d_{xy}-\pi_x^*}\pi^{*1}_{\pi_z^*-d_{yz}}\right)$	11.2	
	$(N^{\wedge}N)_mCu(O_2)$		
ground state ($^1A'$)	$\pi^{2}_{\pi_z^*+d_{yz}}\delta^{2}_{\pi_x^*+d_{xy}}d^{2}_{y^2-z^2}d^{2}_{x^2}d^{2}_{xz}\delta^{*2}_{d_{xy}-\pi_x^*}\pi^{*0}_{\pi_z^*-d_{yz}}$	54.1	0.0
	$\left(\pi^{1}_{\pi_z^*+d_{yz}}\delta^{2}_{\pi_x^*+d_{xy}}d^{2}_{y^2-z^2}d^{2}_{x^2}d^{2}_{xz}\delta^{*2}_{d_{xy}-\pi_x^*}\pi^{*1}_{\pi_z^*-d_{yz}}\right)$	13.8	
first excited state ($^1A''$)	$\pi^{2}_{\pi_z^*+d_{yz}}\delta^{1}_{\pi_x^*+d_{xy}}d^{2}_{y^2-z^2}d^{2}_{x^2}d^{2}_{xz}\delta^{*2}_{d_{xy}-\pi_x^*}\pi^{*1}_{\pi_z^*-d_{yz}}$	54.6	14.4
	$\left(\pi^{1}_{\pi_z^*+d_{yz}}\delta^{1}_{\pi_x^*+d_{xy}}d^{2}_{y^2-z^2}d^{2}_{x^2}d^{2}_{xz}\delta^{*2}_{d_{xy}-\pi_x^*}\pi^{*2}_{\pi_z^*-d_{yz}}\right)$	19.4	
	$(N^{\wedge}N)_mCo(O_2)$		
ground state ($^3A'$)	$\pi^{2}_{\pi_z^*+d_{yz}}\delta^{2}_{\pi_x^*+d_{xy}}d^{2}_{y^2-z^2}d^{2}_{x^2}d^{1}_{xz}\delta^{*1}_{d_{xy}-\pi_x^*}\pi^{*0}_{\pi_z^*-d_{yz}}$	66.6	0.0
	$\left(\pi^{0}_{\pi_z^*+d_{yz}}\delta^{2}_{\pi_x^*+d_{xy}}d^{2}_{y^2-z^2}d^{2}_{x^2}d^{1}_{xz}\delta^{*1}_{d_{xy}-\pi_x^*}\pi^{*2}_{\pi_z^*-d_{yz}}\right)$	5.0	
first excited state ($^3A''$)	$\pi^{2}_{\pi_z^*+d_{yz}}\delta^{2}_{\pi_x^*+d_{xy}}d^{2}_{y^2-z^2}d^{1}_{x^2}d^{1}_{xz}\delta^{*2}_{d_{xy}-\pi_x^*}\pi^{*0}_{\pi_z^*-d_{yz}}$	30.9	4.0
	$\left(\pi^{2}_{\pi_z^*+d_{yz}}\delta^{2}_{\pi_x^*+d_{xy}}d^{1}_{y^2-z^2}d^{2}_{x^2}d^{2}_{xz}\delta^{*1}_{d_{xy}-\pi_x^*}\pi^{*0}_{\pi_z^*-d_{yz}}\right)$	17.8	
second excited state ($^3A''$)	$\pi^{2}_{\pi_z^*+d_{yz}}\delta^{2}_{\pi_x^*+d_{xy}}d^{2}_{y^2-z^2}d^{1}_{x^2}d^{2}_{xz}\delta^{*1}_{d_{xy}-\pi_x^*}\pi^{*0}_{\pi_z^*-d_{yz}}$	27.1	5.6
	$\left(\pi^{2}_{\pi_z^*+d_{yz}}\delta^{2}_{\pi_x^*+d_{xy}}d^{1}_{y^2-z^2}d^{2}_{x^2}d^{2}_{xz}\delta^{*1}_{d_{xy}-\pi_x^*}\pi^{*0}_{\pi_z^*-d_{yz}}\right)$	22.0	
	$(Me_3P)_2Ni(O_2)$		
ground state ($^1A'$)	$\pi^{2}_{\pi_z^*+d_{yz}}\delta^{2}_{\pi_x^*+d_{xy}}d^{2}_{y^2-z^2}d^{2}_{x^2}d^{2}_{xz}\delta^{*2}_{d_{xy}-\pi_x^*}\pi^{*0}_{\pi_z^*-d_{yz}}$	64.5	0.0
	$\left(\pi^{1}_{\pi_z^*+d_{yz}}\delta^{2}_{\pi_x^*+d_{xy}}d^{2}_{y^2-z^2}d^{2}_{x^2}d^{2}_{xz}\delta^{*2}_{d_{xy}-\pi_x^*}\pi^{*1}_{\pi_z^*-d_{yz}}\right)$	5.9	
first excited state ($^1A''$)	$\pi^{2}_{\pi_z^*+d_{yz}}\delta^{1}_{\pi_x^*+d_{xy}}d^{2}_{y^2-z^2}d^{2}_{x^2}d^{2}_{xz}\delta^{*2}_{d_{xy}-\pi_x^*}\pi^{*1}_{\pi_z^*-d_{yz}}$	55.9	19.1
	$\left(\pi^{1}_{\pi_z^*+d_{yz}}\delta^{1}_{\pi_x^*+d_{xy}}d^{2}_{y^2-z^2}d^{2}_{x^2}d^{2}_{xz}\delta^{*2}_{d_{xy}-\pi_x^*}\pi^{*2}_{\pi_z^*-d_{yz}}\right)$	12.3	

structure is 0.2 kcal mol^{-1} lower than the C_{2V} symmetry one like in the real complex. From the results above, it is concluded that the symmetry reduction does not arise from the steric effect but from the electronic factor, which will be discussed below. In

dx.doi.org/10.1021/ic402059b | Inorg. Chem. 2013, 52, 13146−13159

addition, the calculated O−O stretching frequency is 1056 cm^{-1}, which is close to the experimental one (971 cm^{-1}),[30] even without a scaling factor. These results also suggest that the model employed here is reasonable and useful for discussion.

We investigated similar dioxygen complexes $(N^{\wedge}N)_mCu(O_2)$, $(N^{\wedge}N)_mCo(O_2)$, and $(Me_3P)_2Ni(O_2)$ for comparison, where the model $(N^{\wedge}N)_m$ ligand was employed. Although $(N^{\wedge}N)Co(O_2)$ has not been reported experimentally, three coordinated Co(I) complexes with the N^N ligand have been synthesized.[61,62] $(N^{\wedge}N)Co(O_2)$ is, hence, a good target of synthesis. The C_{2V}-optimized geometries of $(N^{\wedge}N)_mCu(O_2)$, $(N^{\wedge}N)_mCo(O_2)$, and $(Me_3P)_2Ni(O_2)$ do not exhibit imaginary frequency unlike $(N^{\wedge}N)_mNi(O_2)$, indicating that their equilibrium structures are C_{2V} symmetrical. In $(N^{\wedge}N)_mCu(O_2)$, the singlet state calculated by the DFT(TPSSTPSS) method is 0.2 kcal mol^{-1} higher than the lowest energy triplet state, similar to the previous reports.[30,40] The CASPT2 calculation by Cramer et al. indicated that the singlet state is the ground state.[34] Our MS-RASPT2 calculation also shows that the singlet state is more stable than the triplet state by 4.5 kcal mol^{-1}. In addition, the O−O bond length (1.393 Å) of $(N^{\wedge}N)_mCu(O_2)$ in the singlet state agrees well with the experimental value (1.392 Å).[32] On the other hand, the O−O bond length of the triplet state is somewhat shorter than the experimental one by 0.067 Å. All these results suggest that $(N^{\wedge}N)_mCu(O_2)$ has a singlet ground state with a C_{2V} symmetrical structure, which will be discussed below with MS-RASPT2 computational results.

$(N^{\wedge}N)_mCo(O_2)$ has a triplet ground state with a C_{2V} symmetrical structure. The closed-shell singlet is 11.1 kcal mol^{-1} higher than the triplet state. The Co−O and O−O distances are 1.800 and 1.405 Å, respectively.[63] Another Ni(0) complex $(Ph_3P)_2Ni^0(O_2)$ was experimentally investigated previously by infrared spectra and equilibrium isotope effects, while no X-ray structure has been reported.[28,29] $(Me_3P)_2Ni(O_2)$ also has a singlet ground state with a C_{2V} symmetrical structure, where PPh_3 was replaced by PMe_3. The Ni−O distance (1.824 Å) is moderately shorter than the average value of $(N^{\wedge}N)_mNi(O_2)$, and the O−O bond length (1.433 Å) is considerably longer than that of $(N^{\wedge}N)_mNi(O_2)$, as expected; remember that the Ni center takes a 0 oxidation state in $(Me_3P)_2Ni$ but +1 oxidation state in $(N^{\wedge}N)_mNi$.

Based on the above results, it is concluded that the symmetry reduction from C_{2V} to C_S occurs only in $(N^{\wedge}N)Ni(O_2)$. The M−O bond becomes longer in the order $(N^{\wedge}N)_mCo(O_2)$ < $(Me_3P)_2Ni(O_2)$ < $(N^{\wedge}N)_mNi(O_2)$ < $(N^{\wedge}N)_mCu(O_2)$, but the O−O bond becomes shorter in the order $(Me_3P)_2Ni(O_2)$ > $(N^{\wedge}N)_mCo(O_2)$ > $(N^{\wedge}N)_mCu(O_2)$ > $(N^{\wedge}N)_mNi(O_2)$. It is of considerable interest that $(N^{\wedge}N)_mNi(O_2)$ has the shortest O−O distance but the medium Ni−O distance. Also, $(N^{\wedge}N)_mCo(O_2)$ has the shortest Co−O distance and the Cu^I analogue has the longest Cu−O distance, while their O−O distances are medium. Since the M−O and O−O bond lengths are closely related to the metal−dioxygen bonding nature, we will examine the bonding nature and the geometrical features of those complexes and explore the reasons in the following section.

Electronic States of $(N^{\wedge}N)_mM(O_2)$ and $(Me_3P)_2Ni(O_2)$. Prior to the discussion of the metal−dioxygen bonding nature, it is necessary to understand the electronic structure of these complexes. The metal−dioxygen interaction often includes an almost-degenerate electronic structure. Previously, a difference dedicated configuration interaction (DDCI) study reported that the doublet ground state of $(N^{\wedge}N)Ni(O_2)$ contains three singly occupied orbitals,[36] but DFT study indicated that the doublet ground state contains one singly occupied orbital.[30] We employed the state-averaged MS-RASPT2 method[64] here to elucidate which description of the electronic state is correct.

In $(N^{\wedge}N)_mNi(O_2)$ with a C_S symmetry, the main configuration of the ground state is $\pi^2_{\pi_z^*+d_{yz}}\delta^2_{\pi_x^*+d_{xy}}d^2_{y^2-z^2}d^2_{x^2}d^2_{xz}\delta^1_{d_{xy}-\pi_x^*}\pi^0_{\pi_z^*-d_{yz}}$, where the subscripts a+b and a−b represent bonding and antibonding combinations between orbitals a and b, respectively, the asterisk symbol (*) is added to the antibonding π orbital of O_2 (not added to a and b), and the superscript is the number of electron in the orbital. Its weight is only 44.1%, as shown in Table 1. The d_{yz} forms a bonding orbital $\pi_{\pi_z^*+d_{yz}}$ and an antibonding orbital $\pi_{\pi_z^*-d_{yz}}$ with the O_2 π_z^* orbital; see Scheme 2.[65] Although the d_{yz} is singly occupied in $(N^{\wedge}N)_mNi$, the $\delta_{\pi_x^*+d_{xy}}$ becomes singly occupied in $(N^{\wedge}N)_mNi(O_2)$. The reason is easily understood by Scheme 2. Because the d_{yz} overlaps well with the O_2 π_z^* orbital, its bonding MO becomes more stable in energy than the $\delta_{\pi_x^*+d_{xy}}$ and its antibonding MO becomes more unstable than the $\delta_{\pi_x^*+d_{xy}}$. Hence, the $\delta_{\pi_x^*+d_{xy}}$ becomes singly occupied. The second leading term is $\pi^2_{\pi_z^*+d_{yz}}\delta^2_{\pi_x^*+d_{xy}}d^2_{y^2-z^2}d^2_{x^2}d^1_{xz}\delta^2_{d_{xy}-\pi_x^*}\pi^0_{\pi_z^*-d_{yz}}$, whose weight is

Scheme 2. Interactions between Metal Orbitals (d_{yz} and d_{xy}) and O_2 π^* Orbitals (π_x^* and π_z^*)[a] in $(N^{\wedge}N)_mNi(O_2)$ as an Example

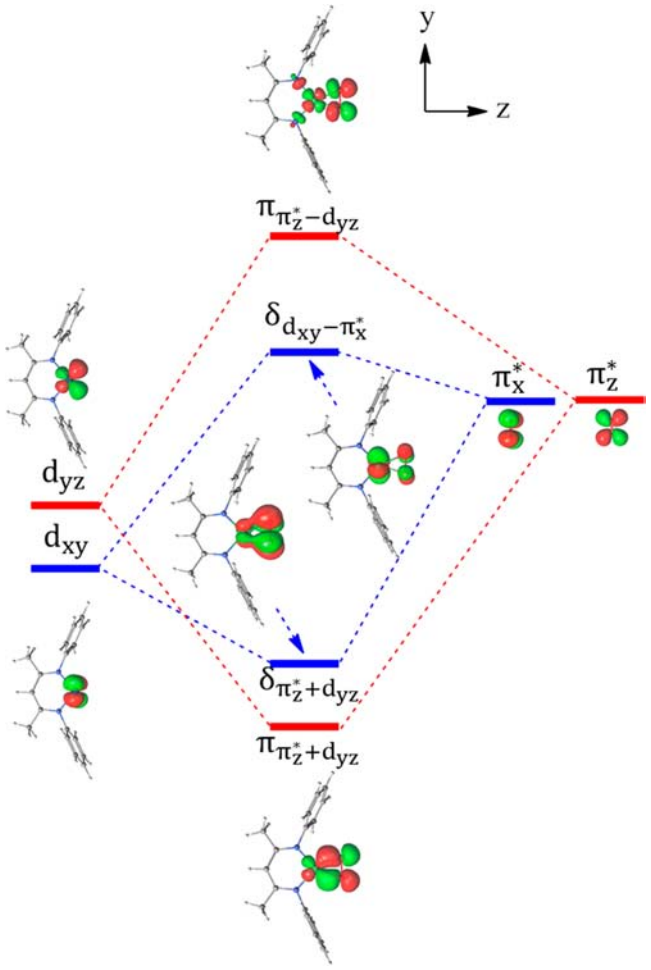

[a]The $\pi_{\pi_z^*+d_{yz}}$ orbital represents the bonding molecular orbital (MO) between the π_z^* orbital of O_2 and the d_{yz} orbital of metal.

dx.doi.org/10.1021/ic402059b | Inorg. Chem. 2013, 52, 13146−13159

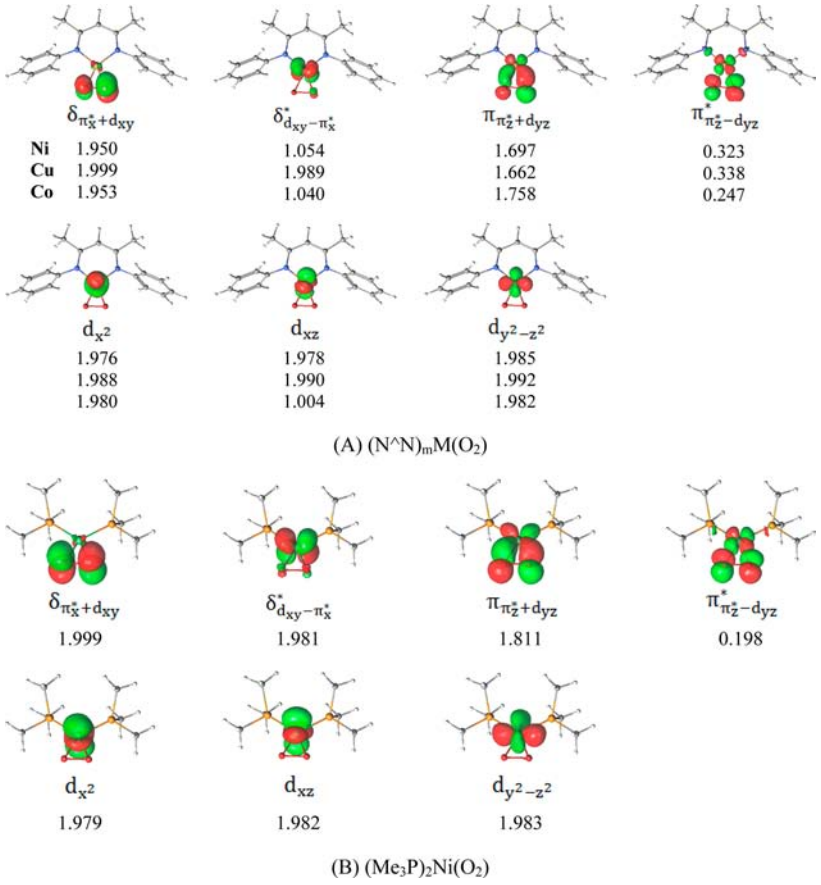

Figure 2. Occupation numbers of natural orbitals of (A) $(N^N)_mM(O_2)$ and (B) $(Me_3P)_2Ni(O_2)$ by the RASSCF method.

17.6%; see Table 1. These results indicate that the static electron correlation is very strong in $(N^N)_mNi(O_2)$. Because the nature of the O_2 moiety cannot be discussed well with the main electron configuration, we employed natural orbitals. As shown in Figure 2, the $\delta_{\pi_x^*+d_{xy}}$ orbital is singly occupied, in which the d_{xy} component is much larger than the O_2 π_x^* component. This means that the spin density is mainly localized on the Ni center. The occupation number of the $\pi_{\pi_z^*+d_{yz}}$ is 1.697 and that of the $\pi_{\pi_z^*-d_{yz}}$ is 0.323, indicating that these two orbitals are responsible for the large electron correlation effect. It is noted that the d_{yz} component is comparable to the O_2 π_z^* in the bonding $\pi_{\pi_z^*+d_{yz}}$ orbital, indicating that the d_{yz} strongly interacts with the O_2 π_z^*, as mentioned above. The remaining three d orbitals, d_{x^2}, d_{xz}, and $d_{x^2-y^2}$, are essentially doubly occupied. If the $\pi_{\pi_z^*+d_{yz}}$ is considered to be formed by the CT from the doubly occupied π_z^* to the empty d_{yz}, the Ni center is understood to be a d^7 system; in other words, it takes a +3 oxidation state in a formal sense and the dioxygen moiety exhibits considerable peroxo character. However, the d_{yz} considerably contributes to the $\pi_{\pi_z^*+d_{yz}}$, which suggests that the Ni center is considered to be intermediate between d^8 and d^7 and the dioxygen moiety exhibits character between peroxo and superoxo. This issue will be discussed below in detail. The singly occupied MO calculated by the DFT is also the $\delta_{\pi_x^*+d_{xy}}$ orbital, but the major component of the $\delta_{\pi_x^*+d_{xy}}$ is the π_x^* of O_2 (see Figure S1 in the Supporting Information). The first and second excited doublet states are 4.3 and 6.1 kcal mol^{-1} higher than the ground state, respectively. The main configuration of the first excited doublet state is $\pi^2_{\pi_z^*+d_{yz}}\delta^2_{\pi_x^*+d_{xy}}d^2_{y^2-z^2}d^2_{x^2}d^1_{xz}\delta^2_{d_{xy}-\pi_x^*}\pi^0_{\pi_z^*-d_{yz}}$ with the weight of 62.9%. In $(N^N)_mNi(O_2)$ with a C_{2V} symmetry structure, the ground, first, and second excited doublet states are essentially the same as those of $(N^N)_mNi(O_2)$ with a C_S symmetry, while the weight of main configuration is somewhat larger than in the C_S symmetry. MS-RASPT2 calculations indicate that the ground state with the C_S symmetry structure is 1.0 kcal mol^{-1} lower than that of the C_{2V} symmetry structure.

In MS-RASPT2 calculations of $(N^N)_mCo(O_2)$ and $(N^N)_mCu(O_2)$, we employed the same active orbitals as those of $(N^N)_mNi(O_2)$, as depicted in Figure S2 in the Supporting Information, where 16 and 18 electrons are involved in the active spaces of the Co and Cu complexes, respectively.[64] The main configuration of the ground state of $(N^N)_mCu(O_2)$ is $\pi^2_{\pi_z^*+d_{yz}}\delta^2_{\pi_x^*+d_{xy}}d^2_{y^2-z^2}d^2_{x^2}d^2_{xz}\delta^2_{d_{xy}-\pi_x^*}\pi^0_{\pi_z^*-d_{yz}}$ with a weight of 54.1%. The second leading configuration is $\pi^1_{\pi_z^*+d_{yz}}\delta^2_{\pi_x^*+d_{xy}}d^2_{y^2-z^2}d^2_{x^2}d^2_{xz}\delta^2_{d_{xy}-\pi_x^*}\pi^1_{\pi_z^*-d_{yz}}$, whose weight is 13.8%. The occupation number of the natural orbitals are similar to those of $(N^N)_mNi(O_2)$, except for the large occupation number (1.989) of the $\delta_{\pi_x^*+d_{xy}}$, which is nearly 1.0 in $(N^N)_mNi(O_2)$. This is because $(N^N)_mCu(O_2)$ has one more d electron than the Ni analogue and it occupies the $\delta_{\pi_x^*+d_{xy}}$ (see Scheme 2). In the $\delta_{\pi_x^*+d_{xy}}$, the contribution of d_{xy} is much larger than that of π_x^*. The $\pi_{\pi_z^*+d_{yz}}$ is similar to that of the Ni analogue. Although the occupation number of the $\delta_{\pi_x^*+d_{xy}}$ is significantly different between the Ni and Cu analogues, the contribution of the O_2 π_x^* is very small in this molecular orbital (MO). Hence, the electronic structure of the Cu–O_2 moiety is similar to that of $(N^N)_mNi(O_2)$. The first

dx.doi.org/10.1021/ic402059b | Inorg. Chem. 2013, 52, 13146–13159

Table 2. Electron Populations of Important MOs of M and O_2 Fragments, and O−O Bond Orders

	$(N^{\wedge}N)_mNi(O_2)$	$(N^{\wedge}N)_mCu(O_2)$	$(N^{\wedge}N)_mCo(O_2)$	$(Me_3P)_2Ni(O_2)$
$p_{d_{yz}}p_{\pi_z}{}^{*a}$	46.9/48.8	53.9/38.5	40.8/52.1	43.8/52.3
$d_{y^2-z^2}$	1.945	1.954	1.917	1.943
d_{x^2}	1.947	1.975	1.962	1.943
d_{xz}	1.702	1.976	1.021	1.967
d_{xy}	1.389	1.979	1.090	1.963
d_{yz}	1.026	1.100	0.874	0.925
σ_{O-O}	1.973	1.975	1.974	1.985
π_x	1.976	1.966	1.953	1.969
π_z	1.926	1.873	1.922	1.917
π_x^*	1.889	1.985	1.875	1.981
π_z^*	1.016	0.960	1.116	1.137
BO_{O-O}	0.499	0.447	0.442	0.384

[a]The percentage of populations ($p_{d_{yz}}$ and $p_{\pi_z^*}$) of the metal d_{yz} and O_2 π_z^* orbitals in $\pi_{\pi_z^*+d_{yz}}$.

singlet excited state is $\pi^2_{\pi_z^*+d_{yz}}\delta^1_{\pi_x^*+d_{xy}}d^2_{y^2-z^2}d^2_{x^2}d^2_{xz}\delta^2_{d_{xy}-\pi_x^*}\pi^1_{\pi_z^*-d_{yz}}$, which is 14.4 kcal mol^{-1} higher in energy than the ground state.

In $(N^{\wedge}N)_mCo(O_2)$, the main configuration of the ground state is triplet $\pi^2_{\pi_z^*+d_{yz}}\delta^2_{\pi_x^*+d_{xy}}d^2_{y^2-z^2}d^2_{x^2}d^1_{xz}\delta^1_{d_{xy}-\pi_x^*}\pi^0_{\pi_z^*-d_{yz}}$ with a weight of 66.6%. The weight of the second leading term, $\pi^0_{\pi_z^*+d_{yz}}\delta^2_{\pi_x^*+d_{xy}}d^2_{y^2-z^2}d^2_{x^2}d^1_{xz}\delta^1_{d_{xy}-\pi_x^*}\pi^2_{\pi_z^*-d_{yz}}$, is only 5.0%. Obviously, two unpaired electrons are localized on the metal center, as shown in Figure 2; in other words, this complex has a metal-centered triplet ground state. The occupation numbers of natural orbitals are similar to those of $(N^{\wedge}N)_mNi(O_2)$ except for the d_{xz}; it is singly occupied in $(N^{\wedge}N)_mCo(O_2)$ but doubly occupied in the Ni(I) analogue. This difference arises from the difference in the number of d electrons. The first triplet excited state, which mainly consists of $\pi^2_{\pi_z^*-d_{yz}}\delta^2_{\pi_x^*-d_{xy}}d^2_{y^2-z^2}d^1_{x^2}d^1_{xz}\delta^2_{d_{xy}-\pi_x^*}\pi^0_{\pi_z^*-d_{yz}}$, is higher than the ground state by 4.0 kcal mol^{-1}. The second triplet excited state, mainly consisting of $\pi^2_{\pi_z^*+d_{yz}}\delta^2_{\pi_x^*+d_{xy}}d^2_{y^2-z^2}d^1_{x^2}d^2_{xz}\delta^1_{d_{xy}-\pi_x^*}\pi^0_{\pi_z^*-d_{yz}}$, is 5.6 kcal mol^{-1} higher in energy than the ground state, where one-electron excitation from d_{x^2} to d_{xz} is involved. Because a significantly large difference is found only in the d_{xz} orbital, the electronic structure of the Co−O_2 moiety is understood to be similar to that of $(N^{\wedge}N)_mNi(O_2)$.

The ground state of $(Me_3P)_2Ni(O_2)$ is singlet, in which the main configuration is $\pi^2_{\pi_z^*+d_{yz}}\delta^2_{\pi_x^*+d_{xy}}d^2_{y^2-z^2}d^2_{x^2}d^2_{xz}\delta^2_{d_{xy}-\pi_x^*}\pi^0_{\pi_z^*-d_{yz}}$ with a weight of 64.5%.[66] The weight of the second leading configuration, $\pi^1_{\pi_z^*+d_{yz}}\delta^2_{\pi_x^*+d_{xy}}d^2_{y^2-z^2}d^2_{x^2}d^2_{xz}\delta^2_{d_{xy}-\pi_x^*}\pi^1_{\pi_z^*-d_{yz}}$, is only 5.9%, which is much smaller than that of $(N^{\wedge}N)_mNi(O_2)$. The occupation numbers of the $\delta_{\pi x}{}^*{}_{+d_{xy}}$ and the $\delta_{d_{xy}-\pi x}{}^*$ are ∼2.0, as shown in Figure 2B, indicating that both the d_{xy} and O_2 π_x^* orbitals have an electron population of 2.0. The occupation numbers of all the natural orbitals are similar to those of $(N^{\wedge}N)_mCu(O_2)$, suggesting that the Ni−O_2 character of $(Me_3P)_2Ni(O_2)$ is similar to that of $(N^{\wedge}N)_mCu(O_2)$. The ground and the first excited singlet states of $(Me_3P)_2Ni(O_2)$ are the same as those of $(N^{\wedge}N)_mCu(O_2)$, while the first vertical excitation energy is considerably large (19.1 kcal mol^{-1}) in $(Me_3P)_2Ni(O_2)$ but moderate (14.4 kcal mol^{-1}) in $(N^{\wedge}N)_mCu(O_2)$.

Based on the above discussion, it is concluded interestingly that the O_2 moiety is understood to be similar in all these complexes, despite different oxidation states and different numbers of d electrons.

At the end of this section, we wish to briefly discuss the C_S symmetry of $(N^{\wedge}N)Ni(O_2)$. In $(N^{\wedge}N)_mNi(O_2)$ with C_{2V} symmetry, the first and second doublet excited states exist slightly above the ground state, where the energy difference is only 1.8 and 2.9 kcal mol^{-1}, respectively (see Table 1). On the other hand, the energy gap in $(N^{\wedge}N)_mCu(O_2)$, $(N^{\wedge}N)_mCo(O_2)$, and $(Me_3P)_2Ni(O_2)$ are 14.4, 4.0, and 19.1 kcal mol^{-1}, respectively, which are larger than in $(N^{\wedge}N)_mNi(O_2)$. More important is the symmetry of the electronic state; in $(N^{\wedge}N)_mNi(O_2)$, both the ground and first excited states belong to A″ irreducible representation under C_S symmetry, while they belong to different irreducible representations in other complexes (see Table 1). Therefore, the symmetry reduction occurs through the pseudo-Jahn−Teller effect in $(N^{\wedge}N)Ni(O_2)$, but it is not observed in the other complexes.

Characterization of the M−O_2 Moiety, Superoxo vs Peroxo. The O_2 moiety strongly interacts with the metal moiety in the $\pi_{\pi_z^*+d_{yz}}$, as seen in Figure 2. In the other natural orbitals, the d orbitals of the metal moiety and the π^* orbitals of the O_2 moiety are well-localized. It is noted that the π_x^* orbital of the O_2 moiety is doubly occupied in all these complexes. If the d_{yz} component is negligibly small in the $\pi_{\pi_z^*+d_{yz}}$ orbital, the dioxygen moiety assumes a charge of nearly −2 in $(N^{\wedge}N)_mNi(O_2)$. In such cases, the O_2 moiety is a pure peroxo species. If the d_{yz} component is comparable to the π_z^* component, the dioxygen moiety assumes a charge of nearly −1, indicating that the O_2 moiety is a pure superoxo species. This understanding is also reasonable in the other three complexes, because the $\delta_{\pi_z^*+d_{yz}}$ is doubly occupied in all of them. In other words, the character of the O_2 moiety is mainly determined by the $\pi_{\pi_z^*+d_{yz}}$. These results mean that the electronic state of the O_2 moiety is understood by analyzing the $\pi_{\pi_z^*+d_{yz}}$.

In general, the MO of complex AB can be represented by a linear combination of MOs of fragments A and B,[67−69] as described by eq 1:

$$\varphi_i^{AB} = \sum_m C_{im}^A \varphi_m^A \sum_n C_{in}^B \varphi_n^B \quad (1)$$

where φ_i^{AB} represents the ith MO of complex AB and φ_m^A and φ_n^B are the mth and nth MOs of fragments A and B, respectively. C_{im}^A and C_{in}^B are expansion coefficients of φ_m^A and φ_n^B, respectively, and the electron populations of φ_m^A and φ_n^B can be obtained from these coefficients. We have successfully used this method to understand the charge-transfer interaction in transition-metal complexes.[70−73] In the present work, the transition-metal−dioxygen complex was divided into the dioxygen moiety and the remaining

dx.doi.org/10.1021/ic402059b | Inorg. Chem. 2013, 52, 13146−13159

moiety, including the transition metal and the other ligand. As shown in Table 2 (the first column), the contribution of the d_{yz} is similar to that of the O_2 π_z^* in the $\pi_{\pi_z^*+d_{yz}}$. Because the d_{yz} participates in the antibonding counterpart $\pi_{\pi_z^*-d_{yz}}$, we evaluated the population of the d_{yz} considering all the natural orbitals. Also, we calculated the electron population ($q_{\pi_z}^*$) of the π_z^* orbital of the O_2 moiety in the same way. The $q_{\pi_z^*}$ is found between 0.96 and 1.14. The total d orbital population is ~7 in $(N^\wedge N)_mCo(O_2)$, ~8 in the Ni analogue, ~9 in the Cu analogue, and ~9 in $(Me_3P)_2Ni(O_2)$.

The O−O π-bond order is one of the important measures for understanding the character of O_2 moiety: peroxo or superoxo. The π-bond order should be zero (0) for peroxo and 0.5 for superoxo. The BO_{O-O} π-bond order is defined by eq 2:

$$BO_{O-O} = \frac{q_{\pi_x} + q_{\pi_z} - q_{\pi_x^*} - q_{\pi_z^*}}{2} \quad (2)$$

where q_{π_x} is the occupation number of the π_x orbital. The π bond order of the O_2 moiety is evaluated to be 0.38 to 0.50 (see Table 2). Based on these results, it is likely concluded that these complexes exhibit a considerable superoxo nature rather than a peroxo nature from the viewpoint of electron distribution.

The superoxo character and the ground-state electronic structure ($^2A_2$) are the same as the previously calculated results by the DDCI method.[36,37] In our calculation, the main configuration of the ground state of $(N^\wedge N)_mNi(O_2)$ is $\pi^2_{\pi_z^*+d_{yz}}\delta^2_{\pi_x^*+d_{xy}}d^2_{y^2-z^2}d^2_{x^2}d^2_{xz}\delta^1_{d_{xy}-\pi_x^*}\pi^0_{\pi_z^*-d_{yz}}$, which contains only one singly occupied orbital $\delta_{\pi_x^*+d_{xy}}$. This electronic state is easily understood in terms of the strong overlap between the π_z^* of O_2 and the d_{yz}. Because of the strong overlap, the $\pi_{\pi_z^*+d_{yz}}$ is much more stabilized in energy than the $\delta_{\pi_x^*+d_{xy}}$ and as a result, its antibonding counterpart $\pi_{\pi_z^*-d_{yz}}$ becomes very unstable in energy, as discussed above and shown in Scheme 2 (see page S14 in the Supporting Information for an understanding of this $^2A_2$ state. In the previous report,[36] the $^2A_2$ ground state is understood to possess mainly the character of $\pi^1_{\pi_z^*+d_{yz}}\delta^2_{\pi_x^*+d_{xy}}d^2_{y^2-z^2}d^2_{x^2}d^2_{xz}\delta^1_{d_{xy}-\pi_x^*}\pi^1_{\pi-d_{yz}z^*}$ consisting of three singly occupied orbitals. We performed four-state-average CASSCF(9e, 6o)/CASPT2 calculation, where the active space was taken as the same as the previous study.[36] The CASPT2 calculation indicates that the ground state is the $^2A_2$ containing $\pi^2_{\pi_z^*+d_{yz}}\delta^2_{\pi_x^*+d_{xy}}d^2_{y^2-z^2}d^2_{x^2}d^2_{xz}\delta^1_{d_{xy}-\pi_x^*}\pi^0_{\pi_z^*-d_{yz}}$ as a main configuration like in the MS-RASPT2 calculation with large active space and the $^2A_2$ containing $\pi^1_{\pi_z^*+d_{yz}}\delta^2_{\pi_x^*+d_{xy}}d^2_{y^2-z^2}d^2_{x^2}d^2_{xz}\delta^1_{d_{xy}-\pi_x^*}\pi^1_{\pi_z^*-d_{yz}}$ as a main configuration is at a much higher energy (87.1 kcal/mol) than the ground state; see page S14 in the Supporting Information for details. Considering the strong overlap between the π_z^* of O_2 and the d_{yz}, it seems reasonable to conclude that the ground state ($^2A_2$) has a main character of $\pi^2_{\pi_z^*+d_{yz}}\delta^2_{\pi_x^*+d_{xy}}d^2_{y^2-z^2}d^2_{x^2}d^2_{xz}\delta^1_{d_{xy}-\pi_x^*}\pi^0_{\pi_z^*-d_{yz}}$.

Although $(N^\wedge N)Cu(O_2)$ and $(N^\wedge N)Ni(O_2)$ exhibit a considerable superoxo nature, the reactivity for hydrogen abstraction from O−H and N−H groups[15,41] is different from the typical end-on η^1-superoxo copper, cobalt, and iron−dioxygen complexes, because the out-of-plane π^* orbital of O_2 is singly occupied in those complexes.[19] In $(N^\wedge N)Cu(O_2)$, the ground state is close-shell singlet and no spin density is found in the O_2 moiety. In $(N^\wedge N)Ni(O_2)$, the unpaired electron is mainly localized in the Ni center; see Figure S2 in the Supporting Information. In addition, the out-of-plane π_x^* is doubly occupied. Thus, the spin density on the O_2 moiety is very small unlike the O_2 moiety in the typical η^1-superoxo complex. It is likely that $(N^\wedge N)Ni(O_2)$ and the Cu analogue exhibit different reactivity from that of the typical η^1-superoxo complex.

Factors Determining the M−O Bond Lengths. Cramer et al. reported that the Mayer bond order of O−O is inversely proportional to the M−O bond order, in which the O−O distance was compared among neutral, superoxo, and peroxo species.[19] Here, all four complexes exhibit considerable superoxo nature in the O_2 moiety, but the M−O bond and O−O distance are considerably different among them; for instance, $(N^\wedge N)_mCu(O_2)$ has the longest M−O bond length (1.846 Å), $(N^\wedge N)_mCo(O_2)$ has the shortest one (1.800 Å), $(Me_3P)_2Ni(O_2)$ has the longest O−O bond length, and $(N^\wedge N)_mNi(O_2)$ has the shortest one (1.347 Å). If we find the relationship between the M−O bond length and the properties of ML (L = $(N^\wedge N)_m$ or $(Me_3P)_2$), it is useful to understanding the nature of the metal−dioxygen complex.

The M−O bond length becomes shorter in the following order: $(N^\wedge N)_mCu(O_2)$ > $(N^\wedge N)_mNi(O_2)$ > $(Me_3P)_2Ni(O_2)$ > $(N^\wedge N)_mCo(O_2)$. The π-type interaction between the metal and the O_2 moieties is much stronger than the δ-type interaction due to the larger orbital overlap in the π-type interaction, as discussed above (also see Scheme 2). Thus, the π-type interaction is one of the important factors for the M−O bond length. The strength of the π-type interaction is represented by the π-type M−O bond order, which is defined by eq 3:

$$BO_{M-O} = \frac{q_{\pi_z^*+d_{yz}} - q_{\pi_z^*-d_{yz}}}{2} \quad (3)$$

where $q_{\pi z^*+d_{yz}}$ and $q_{\pi z^*-d_{yz}}$ are the occupation numbers of the bonding $\pi_{\pi z^*+d_{yz}}$ and the antibonding $\pi_{\pi z^*-d_{yz}}$ orbitals calculated by the RASSCF method, respectively (see Table S2 in the Supporting Information). Although a good correlation is observed between the M−O bond length and the BO_{M-O} in $(N^\wedge N)_mM(O_2)$ (M = Co, Ni, or Cu), the Ni−O distance of $(Me_3P)_2Ni(O_2)$ largely deviates from the relation, as shown in Figure 3A. Because it is likely that this discrepancy arises from the difference in ionic radii between Ni^+ and Ni^{2+}, we employed another parameter to take the difference in ionic radius into account, as shown in eq 4:

$$R_{M-O}^{correct} = R_{M-O} - \Delta R_{M^{n+}} \quad (4)$$

where R_{M-O} is the M−O bond length in the complex and $\Delta R_{M^{n+}}$ is the difference of ionic radius of M^{n+} from that of Ni^{2+},[74,75] as defined by eq 5.

$$\Delta R_{M^{n+}} = R_{M^{n+}} - R_{Ni^{2+}} \quad (5)$$

where "n+" is the oxidation state. We found a good linear relationship between the BO_{M-O} and the $R_{M-O}^{correct}$, as shown in Figure 3B; in other words, the M−O bond length with correction of ionic radius, rather than the M−O bond length, well relates to the metal−dioxygen interaction.

The next step is to clarify the factor determining the BO_{M-O}. In these dioxygen complexes, the charge transfer mainly occurs from the d_{yz} to the π_z^* orbital of the O_2 moiety via the π-type interaction (Scheme 2). The strength of CT can be evaluated by the electron populations of donor and acceptor MOs, which are evaluated with eq 1, as described in Table 2. One can expect that the M−O_2 bonding interaction becomes stronger and the BO_{M-O} becomes larger, as the CT from the metal d orbital to the

dx.doi.org/10.1021/ic402059b | Inorg. Chem. 2013, 52, 13146−13159

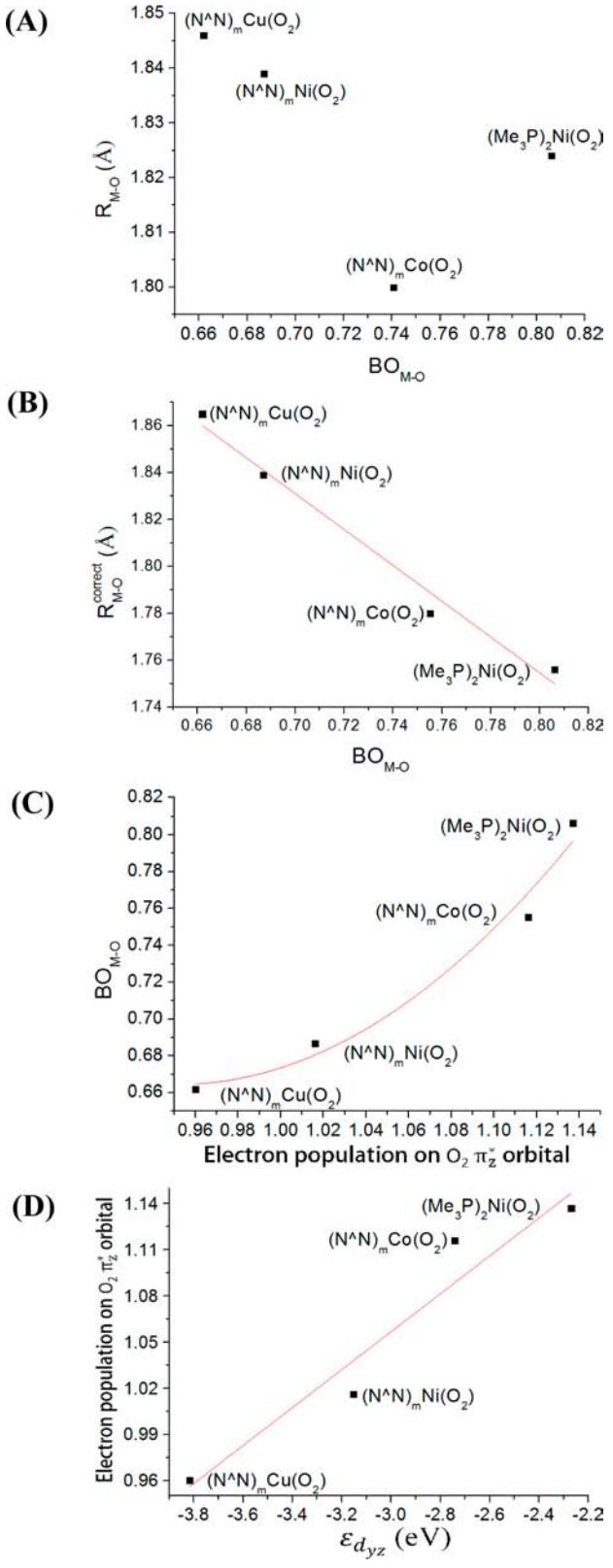

Figure 3. Correlations of (A) R_{M-O} vs BO_{M-O}, (B) $R^{correct}_{M-O}$ vs BO_{M-O}, (C) BO_{M-O} vs the electron population on O_2 π^*_z, and (D) the electron population on O_2 π^*_z vs $\varepsilon_{d_{yz}}$.

O_2 π^*_z increases. As expected, we found a linear relationship between the electron population of the O_2 π^*_z and the BO_{M-O} (see Figure 3C). Because the metal d_{yz} orbital mainly participates in the charge transfer as a donating MO, we calculated the d_{yz} orbital energy ($\varepsilon_{d_{yz}}$) in the valence state.[76] As shown in Figure 3D, a linear relationship between the $\varepsilon_{d_{yz}}$ and the electron population of the O_2 π^*_z orbital is found.

The above results encourage us to examine the relationship between the $\varepsilon_{d_{yz}}$ and the binding energy (E_{BE}). However, we could not find a good relationship between E_{BE} and the $\varepsilon_{d_{yz}}$, as shown by a black line in Figure 4A, where we employed the DFT-

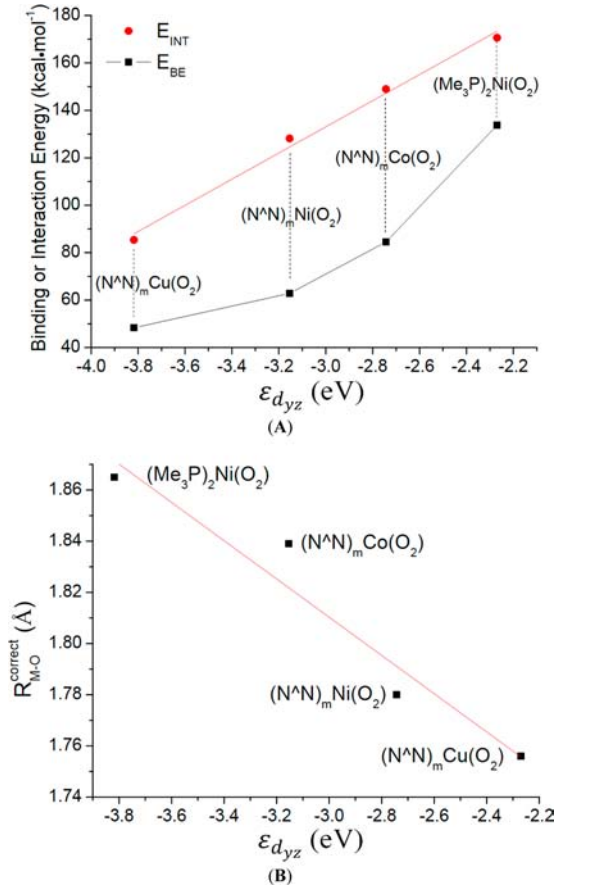

Figure 4. Correlations of (A) E_{BE} and E_{INT} vs $\varepsilon_{d_{yz}}$ and (B) $R^{correct}_{M-O}$ vs $\varepsilon_{d_{yz}}$.

computational results, since the orbital energy cannot be defined by the RASSCF calculation. We must remember that the d_{yz} orbital energy is calculated in the valence state and, hence, it is different from that in the ground state. This means that $\varepsilon_{d_{yz}}$ must be plotted against the interaction energy (E_{INT}), which is the relative energy of $LM(O_2)$ to the sum of ML and O_2 in their valence states. Here, we considered the valence states in both the ML and O_2 moieties. In the O_2 moiety, the valence state is $\pi^{*2}_x\pi^{*0}_z$, which corresponds to the closed-shell singlet state. In $(N^\wedge N)_mCu$ and $(Me_3P)_2Ni$, the ground state is the same as the valence state $d^2_{y^2-z^2}d^2_{x^2}d^2_{xz}d^2_{xy}d^2_{yz}$. In $(N^\wedge N)_mNi$, the valence state is $d^2_{y^2-z^2}d^2_{x^2}d^2_{xz}d^2_{xy}d^1_{yz}$. In $(N^\wedge N)_mCo$, the valence state is $d^2_{y^2-z^2}d^2_{x^2}d^1_{xz}d^1_{xy}d^2_{yz}$. Their energies were calculated with the DFT method (Table 3). As expected, the calculated ΔE_{INT} value linearly increases as the $\varepsilon_{d_{yz}}$ increases; see the red line in Figure 4A. This linear relationship is useful to understand the relationship between E_{BE} and $\varepsilon_{d_{yz}}$, because E_{BE} is represented by E_{INT}, as follows:

dx.doi.org/10.1021/ic402059b | Inorg. Chem. 2013, 52, 13146−13159

Table 3. Orbital Energy ($\varepsilon_{d_{yz}}$), Promotion Energy (E_{prom}), Binding Energy (E_{BE}), Interaction Energy (E_{INT}) Electron Configurations of the Ground and Valence States of the Metal Moiety with Associated Ligand

		E_{prom}				configuration	
	$\varepsilon_{d_{yz}}$ (eV)	ML[a]	O_2	E_{BE} (kcal mol^{-1})	E_{INT} (kcal mol^{-1})	ground state	valence state
$(N^\wedge N)_mNi(O_2)$	−3.2	28.1 (23.0)	37.2	53.3	81.4	$d^2_{y^2-z^2}d^2_{x^2}d^2_{xz}d^2_{xy}d^1_{yz}$	$d^2_{y^2-z^2}d^2_{x^2}d^2_{xz}d^1_{xy}d^2_{yz}$
$(PMe_3)_2Ni(O_2)$	−2.3	0.0	36.8	111.1	111.1	$d^2_{y^2-z^2}d^2_{x^2}d^2_{xz}d^2_{xy}d^2_{yz}$	$d^2_{y^2-z^2}d^2_{x^2}d^2_{xz}d^2_{xy}d^2_{yz}$
$(N^\wedge N)_mCu(O_2)$	−3.8	0.0	37.0	32.3	32.3	$d^2_{y^2-z^2}d^2_{x^2}d^2_{xz}d^2_{xy}d^2_{yz}$	$d^2_{y^2-z^2}d^2_{x^2}d^2_{xz}d^2_{xy}d^2_{yz}$
$(N^\wedge N)_mCo(O_2)$	−2.7	27.5 (12.7)	37.0	66.6	94.0	$d^2_{y^2-z^2}d^2_{x^2}d^2_{xz}d^1_{xy}d^1_{yz}$	$d^2_{y^2-z^2}d^2_{x^2}d^2_{xz}d^1_{xy}d^2_{yz}$

[a]L = $(N^\wedge N)_m$ and $(Me_3P)_2$, and the value in parentheses is calculated by MS-RASPT2.

$$E_{BE} = E[ML]_G + E[O_2]_G - E[ML(O_2)]_G \quad (6)$$

$$= E_{INT} - E_{prom}[ML] - E_{prom}[O_2] \quad (7)$$

where the subscript G represents a ground state and E_{prom} is a promotion energy from the ground state to the valence state; in other words, the linear relationship between E_{INT} and $\varepsilon_{d_{yz}}$ suggests that E_{BE} largely depends on $\varepsilon_{d_{yz}}$ in the valence state and the promotion energy of the ML moiety; remember that the promotion energy of the O_2 moiety is not different very much among these complexes (Table 2). Thus, the difference between E_{BE} and E_{INT} mainly comes from the promotion energy of the ML moiety. Because the d_{yz} orbital of $(Me_3P)_2Ni(O_2)$ is calculated at the highest energy among these complexes, its E_{INT} value is the largest. In addition, the promotion energy is zero in this complex; hence, the E_{BE} value is the largest. In $(N^\wedge N)_mCo(O_2)$, the d_{yz} is calculated at the second highest energy, while in $(N^\wedge N)_mNi(O_2)$ the d_{yz} is lower than in the Co analogue. However, the promotion energies are considerably large in these two complexes (~28 kcal mol^{-1}). In $(N^\wedge N)_mCu(O_2)$, the energy of d_{yz} is the lowest but the promotion energy is zero. Because of the difference in promotion energy, the E_{BE} values of $(N^\wedge N)_mCo(O_2)$ and the Ni analogue are smaller than in $(N^\wedge N)_mCu(O_2)$ and $(Me_3P)_2Ni(O_2)$. Considering these promotion energies, we can easily understand the parabolic relation between $\varepsilon_{d_{yz}}$ and E_{BE} in Figure 4A; the similar relationship is presented when we employed the MS-RASPT2 to evaluate the promotion energy, as shown in Table S3 and Figure S7 in the Supporting Information . Because the $R^{correct}_{M-O}$ is value closely related to the bond strength between metal and O_2, a good relationship between the $R^{correct}_{M-O}$ and the $\varepsilon_{d_{yz}}$ is also found, as shown in Figure 4B. Therefore, the d_{yz} orbital energy is one important factor in determining the M−O bond length and bond strength, as expected.

It is likely concluded that (i) the trend of the M−O bond length largely depends on the d_{yz} orbital energy in the distorted ML moiety with valence state and (ii) the binding energy largely depends on the d_{yz} orbital energy and the promotion energy to the valence state; note that the binding energy also depends on some other factors such as the electrostatic interaction, steric repulsion, and exchange repulsion.

Factors Determining the O−O Bond Length. The O−O bond length is an important geometrical parameter in metal−dioxygen complexes. Although all four of these complexes exhibit similar M−O_2 character, the O−O distance is considerably different, as mentioned above. It is of considerable importance to clarify the factors to determine the O−O distance.

Previously, the inverse correlation was found between the O−O and the M−O distances and between their bond orders.[18,19] However, such a relationship cannot be found in these four complexes. Here, the relationship between the $R^{correct}_{M-O}$ and the O−O distance is examined first because the $R^{correct}_{M-O}$ provides a linear relationship with the BO_{M-O}. However, a linear relationship is not presented between the $R^{correct}_{M-O}$ and the O−O distance, as shown in Figure 5A. For instance, the O−O distance of $(N^\wedge N)_mCu(O_2)$ is much longer than that of $(N^\wedge N)_mNi(O_2)$, despite the shorter $R^{correct}_{M-O}$.

Because the $\varepsilon_{d_{yz}}$ was successfully employed for discussing the E_{INT} and the M−O values, as shown in Figures 5A and 5B, we examined the relationship between the $\varepsilon_{d_{yz}}$ and the O−O distance. However, we also could not find a linear relationship; for instance, the d_{yz} orbital exists at a higher energy in $(N^\wedge N)_mNi$ than in $(N^\wedge N)_mCu$, but the O−O distance of $(N^\wedge N)_mNi(O_2)$ is considerably shorter than that of $(N^\wedge N)_mCu(O_2)$.

One can expect that the O−O distance depends on the electron population of the O_2 moiety (q_{O_2}), because the O−O distance becomes longer as the electron population increases in the π^*_x and π^*_z orbitals. However, a linear relation is not found between them again, as shown in Figure 5B. In this case, the O−O distance of $(N^\wedge N)_mNi(O_2)$ substantially deviates from the relationship; for instance, the q_{O_2} of $(N^\wedge N)_mNi(O_2)$ (−0.845 e) is moderately more negative than that of $(N^\wedge N)_mCu(O_2)$ (−0.815 e), while the O−O distance of the former is much shorter than of the latter. The absence of a linear relationship between the q_{O_2} and O−O distance is attributed to the presence of various CT interactions. For instance, the CT from the metal d_{yz} to the O_2 π^*_z increases both the q_{O_2} value and the O−O distance, as expected. However, the O_2 moiety has a $\pi^{*2}_x\pi^0_z$ configuration in the valence state. This means that the CT can occur from the O_2 π^*_x to the M d_{xy} when the d_{xy} is not doubly occupied. This CT decreases the q_{O_2} value and decreases the O−O distance. When the d_{xz} is unoccupied or singly occupied, the CT occurs from the O_2 π_x to the d_{xz}. Such CT decreases the q_{O_2} but increases the O−O distance, because the electron population decreases in the bonding MO. In $(N^\wedge N)_mNi(O_2)$ and $(N^\wedge N)_mCo(O_2)$, the electron population of the O_2 π^*_x is 1.889 and 1.875, respectively, which are somewhat smaller than that in $(N^\wedge N)_mCu(O_2)$ and $(Me_3P)Ni(O_2)$. Consistent with those populations, the d_{xy} electron populations are 1.389 and 1.090 in $(N^\wedge N)_mNi(O_2)$ and $(N^\wedge N)_mCo(O_2)$, respectively. The larger electron population of the d_{xy} in $(N^\wedge N)_mNi(O_2)$ arises from the CT from the O_2 π^*_x and the configuration mixing between $\pi^2_{\pi^*_z+d_{yz}}\delta^2_{\pi^*_x+d_{xy}}d^2_{y^2-z^2}d^2_{x^2}d^2_{xz}\delta^1_{d_{xy}-\pi^*_x}\pi^0_{\pi^*_z-d_{yz}}$ (41.1%) and

dx.doi.org/10.1021/ic402059b | Inorg. Chem. 2013, 52, 13146−13159

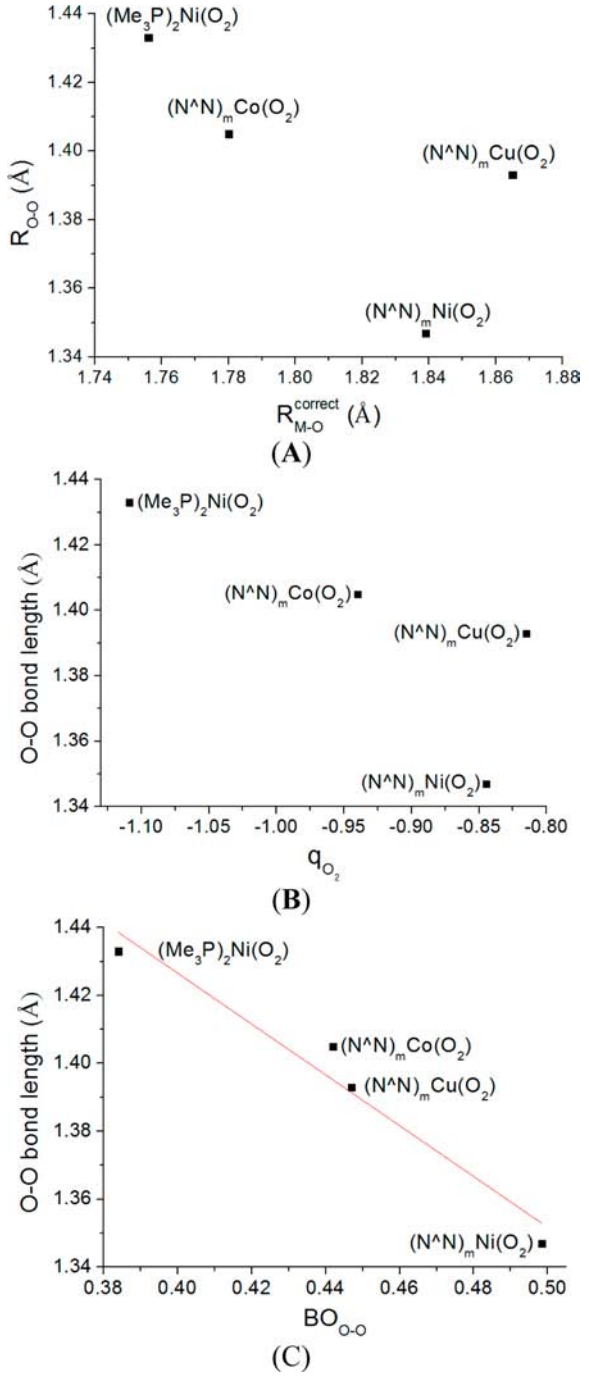

Figure 5. Correlations of the O−O bond length vs (A) $BO_{M\text{-}O}$, (B) Mulliken charge of O_2, and (C) O−O bond order (BO_{O-O}). [The Mulliken charge has been calculated by the RASSCF.]

$\pi^2_{\pi_z^*+d_{yz}}\delta^2_{\pi_x^*+d_{xy}}d^2_{y^2-z^2}d^2_{x^2}d^1_{xz}\delta^2_{d_{xy}-\pi_x^*}\pi^0_{\pi_z^*-d_{yz}}$ (17.6%) in the ground state. In $(N^{\wedge}N)_mCo(O_2)$, the singly occupied d_{xz} orbital induces the CT from the O_2 π_x, which decreases the q_{O_2} value but increases the O−O distance, as mentioned above. These results suggest that we cannot simply discuss the O−O distance based on the q_{O_2} but must consider populations of all π and π^* orbitals. Finally, we employed the O−O π bond order (BO_{O-O}), which is defined by eq 2. Apparently, a linear relationship is presented between the BO_{O-O} and the O−O bond distance, as shown in Figure 5C.

It should be concluded that not only the electron population of the O_2 π_x^* and π_z^* orbitals but also those of the O_2 π_x and π_z orbitals are important to understand the O−O distance, when the metal center has several singly occupied and/or unoccupied d orbital.

Reactivities of $(N^{\wedge}N)_mM(O_2)$ and $(Me_3P)_2Ni(O_2)$. One of the important features of these dioxygen complexes is the reactivity to organic substrates.[22,77−81] Here, the reaction between these dioxygen complexes and phenol was investigated, since substituted phenols are usually employed as substrate for the H atom abstraction reaction by transition-metal−dioxygen complexes;[82,83] actually, the reactions of substituted phenol with $(N^{\wedge}N)Ni(O_2)$[41] and $(N^{\wedge}N)Cu(O_2)$[42] have been experimentally investigated, in which $LM(O_2)$ abstracts the hydroxyl hydrogen of phenol to produce radical $PhO^{\bullet}$ and LM−OOH, as shown below:

$$LM(O_2) + PhOH \rightarrow TS^1 \rightarrow LM - OOH + PhO^{\bullet}$$

The Gibbs activation energy is calculated to be 20.7 kcal/mol in the reaction of $(N^{\wedge}N)_mNi(O_2)$ (see Figure 6 and Table S4 in the Supporting Information). This moderate barrier is consistent with the experimental report that $(N^{\wedge}N)_mNi(O_2)$ is reactive for the hydrogen abstraction reaction.[41] The Gibbs activation energy with $(N^{\wedge}N)_mCu(O_2)$ is 17.1 kcal/mol, which indicates that $(N^{\wedge}N)_mCu(O_2)$ is also reactive for the hydrogen abstraction reaction. However, $(N^{\wedge}N)_mCu(O_2)$ was experimentally reported to be inert toward phenol.[42] We noticed that a very low reaction temperature (−60 °C) was employed in the experiment.[42] It is likely that the reaction with the Gibbs activation energy of 17.1 kcal/mol occurs very slowly at such a low temperature. In addition, $(N^{\wedge}N)_mCu(O_2)$ was experimentally reported to be easily decomposed upon warming.[42] One reasonable understanding is that the decomposition of $(N^{\wedge}N)_mCu(O_2)$ occurs easier than the hydrogen abstraction and, hence, no reactivity was observed for $(N^{\wedge}N)_mCu(O_2)$. However, we wish to stop this discussion, because we do not have computational results about the decomposition; note that the decomposition reaction is complicated in many cases.

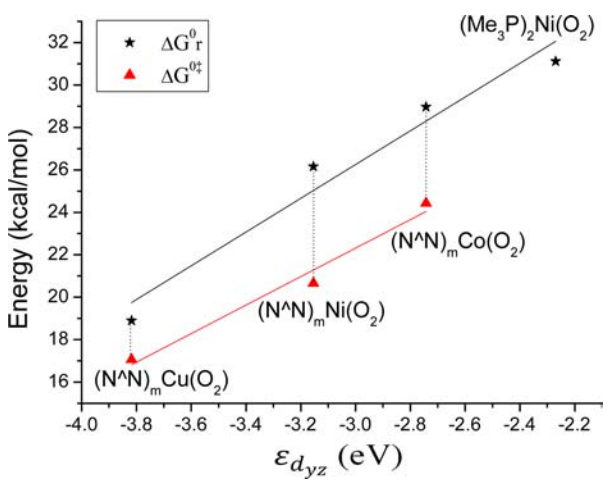

Figure 6. Correlations of ΔG_r vs $\varepsilon_{d_{yz}}$, and $\Delta G^{\ddagger}$ vs $\varepsilon_{d_{yz}}$.

In the hydrogen abstraction reaction by $(N^{\wedge}N)_mCo(O_2)$, the Gibbs activation energy is evaluated to be 24.4 kcal/mol, which is higher than that for $(N^{\wedge}N)_mNi(O_2)$, indicating it is less reactive than the Ni analogue. In the reaction by $(Me_3P)_2Ni(O_2)$, neither radical product $(Me_3P)_2NiOOH\cdots OPh$ nor the transition state for hydrogen abstraction could be located unlike those of $(N^{\wedge}N)_mNi(O_2)$, suggesting that this complex is inert for the

dx.doi.org/10.1021/ic402059b | Inorg. Chem. 2013, 52, 13146−13159

hydrogen abstraction from phenol. The Gibbs reaction energy for $(Me_3P)_2Ni(OOH)$ + •OPh is evaluated to be 31.1 kcal/mol, which is more endothermic than that for $(N^\wedge N)_mNi(OOH)$ + •OPh.

We found the linear relationships between the Gibbs activation energy ($\Delta G^{\ddagger}$) of hydrogen abstraction and the $\varepsilon_{d_{yz}}$ and between the Gibbs reaction energy (ΔG_r) and the $\varepsilon_{d_{yz}}$, as shown in Figure 6. In the previous section, we found that the higher $\varepsilon_{d_{yz}}$ leads to the larger interaction energy (see Figure 4A). These results indicate that high $\varepsilon_{d_{yz}}$ values lead to too strong of a n interaction between O_2 and ML, which is not favorable for the reactivity of the dioxygen complex; in other words, if we employ the appropriate ligand in the Ni(0)−dioxygen complex to stabilize its $\varepsilon_{d_{yz}}$, we can increase its reactivity toward the hydrogen abstraction reaction. However, if $\varepsilon_{d_{yz}}$ is too low, the dioxygen complex becomes too unstable and, hence, some decomposition reactions occur easier, such as $(N^\wedge N)_mCu(O_2)$, which is not favorable.

CONCLUSIONS

Both density functional theory (DFT) and multi-configurational second-order perturbation (MS-RASPT2) calculations clearly show that $(N^\wedge N)Ni(O_2)$ is not C_{2V} but C_S symmetry with different Ni−O bond lengths, which arises from the pseudo-Jahn−Teller effect. On the other hand, $(N^\wedge N)_mCu(O_2)$, $(N^\wedge N)_mCo(O_2)$, and $(Me_3P)_2Ni(O_2)$ all have a C_{2V} symmetry structure in the ground state. The pseudo-Jahn−Teller effect occurs only in $(N^\wedge N)Ni(O_2)$, because of the presence of the singly occupied $\delta_{\pi_x^*+d_{xy}}$ orbital.

MS-RASPT2 calculations disclose that these complexes exhibit considerable superoxo (O_2^-) nature, independent of the metal oxidation state and the number of d electrons. In these complexes, however, little spin density is found on the O_2 moiety since the out-of-plane π^* orbital is doubly occupied and the in-plane π^* orbital strongly interacts with the metal d_{yz} in the doubly occupied bonding orbital. This feature is completely different from the usual η^1-superoxo complex, which possesses one unpaired electron on the O_2 moiety. This would be a reason for different reactivity of these complexes from that of the usual η^1-superoxo complex. This result suggests that we need a new index for discussing the metal−dioxygen interaction besides peroxo, superoxo, and oxo species.

Although all these complexes have a similar metal−dioxygen moiety, their M−O and O−O distances are considerably different among them. We introduced a new parameter, $R_{M-O}^{correct}$, to take the difference of ionic radius of metal center into account, and we found that the $R_{M-O}^{correct}$ linearly correlates to the bond order BO_{M-O} between the metal center and the O_2 moiety. Also, we found that the interaction energy E_{INT} of the dioxygen molecule with the metal moiety linearly correlates to the d_{yz} orbital energy ($\varepsilon_{d_{yz}}$) in the valence state; in other words, as the $\varepsilon_{d_{yz}}$ becomes higher, the $R_{M-O}^{correct}$ decreases and the interaction energy (E_{INT}) increases. It is concluded that the binding energy (E_{BE}) of the dioxygen molecule is determined by the $\varepsilon_{d_{yz}}$ in the valence state and the promotion energy of ML to the valence state.

The O−O bond length is influenced not only by the charge transfer (CT) from ML to O_2 but also by the CT from O_2 π^* and π to ML. Because of the presence of various CTs, the electron population of the O_2 moiety is not a good index for the O−O bond distance. In the present work, we proposed an O−O π bond order (BO_{O-O}) of the O_2 moiety as a good index for the O−O distance, which is calculated using the RASSCF method. Actually, this BO_{O-O} reversely correlates to the O−O bond length.

The calculated Gibbs energy barriers of hydrogen abstraction from phenol suggest that $(N^\wedge N)_mNi(O_2)$ and $(N^\wedge N)_mCo(O_2)$ are reactive toward phenol but $(Me_3P)_2Ni(O_2)$ is not. The reactivity of dioxygen complex exhibits interesting relationship with the d_{yz} orbital energy of ML (L = $(N^\wedge N)$ or $(PMe_3)_2$). Our computational results suggest that $(N^\wedge N)_mCu(O_2)$ is reactive toward phenol if the decomposition reaction is suppressed.

All these reasonable relationships proposed in our work provide clear and well understanding of the nature of the metal-dioxygen moiety and the interaction between the metal and the dioxygen molecule.

ASSOCIATED CONTENT

Supporting Information

Comparison among the structures of $(N^\wedge N)Ni(O_2)$ optimized by various DFT functionals and experimental one (Table S1); the reason why $(N^\wedge N)Ni(O_2)$ takes C_S symmetrical structures (Figure S1); spin density in $(N^\wedge N)Ni(O_2)$ calculated by TSPPTPSS and B3LYP, and singly occupied molecular orbital of $(N^\wedge N)Ni(O_2)$ calculated by TSPPTPSS (Figure S2); the orbitals involved in the active space (Figure S3); the natural orbitals of ML, O_2, and $LM(O_2)$ (M = Co, Cu, and Ni(0)) (Figures S4 and S5); the structures of intermediates and transition states involved in the hydrogen abstracting reaction (Figure S8); the occupation numbers of natural orbital calculated by RASSCF (Table S2); the correlations of the $\varepsilon_{d_{yz}}$ with the E_{BE} and E_{INT} calculated by MS-RASPT2 (Table S3); complete ref 55. This material is available free of charge via the Internet at http://pubs.acs.org.

AUTHOR INFORMATION

Corresponding Author

*Tel.: +81-75-711-7907. Fax: +81-75-711-4757. E-mail: sakaki.shigeyoshi.47e@st.kyoto-u.ac.jp.

Notes

The authors declare no competing financial interest.

ACKNOWLEDGMENTS

This work is financially supported by Grants-in-Aid from the Ministry of Education, Culture, Science, Sport, and Technology through Grants-in-Aid of Specially Promoted Science and Technology (Grant 22000009) and Grand Challenge Project (IMS, Okazaki, Japan). We are also thankful to the computational facility at the Institute of Molecular Science, Okazaki, Japan.

REFERENCES

(1) Klotz, I. M.; Kurtz, D. M. *Chem. Rev.* **1994**, *94*, 567.
(2) Nam, W. *Acc. Chem. Res.* **2007**, *40*, 465.
(3) Kieber-Emmons, M. T.; Riordan, C. G. *Acc. Chem. Res.* **2007**, *40*, 618.
(4) Yao, S.; Driess, M. *Acc. Chem. Res.* **2012**, *45*, 276.
(5) Bollinger, J. M., Jr.; Krebs, C. *Curr. Opin. Chem. Biol.* **2007**, *11*, 151.
(6) Kovaleva, E. G.; Lipscomb, J. D. *Science* **2007**, *316*, 453.
(7) Mirica, L. M.; Ottenwaelder, X.; Stack, T. D. P. *Chem. Rev.* **2004**, *104*, 1013.
(8) Cramer, C. J.; Kinal, A.; Włoch, M.; Piecuch, P.; Gagliardi, L. *J. Phys. Chem. A* **2006**, *110*, 11557.

(9) Cramer, C. J.; Smith, B. A.; Tolman, W. B. *J. Am. Chem. Soc.* **1996**, *118*, 11283.
(10) Cramer, C. J.; Włoch, M.; Piecuch, P.; Puzzarini, C.; Gagliardi, L. *J. Phys. Chem. A* **2006**, *110*, 1991.
(11) Flock, M.; Pierloot, K. *J. Phys. Chem. A* **1998**, *103*, 95.
(12) Malmqvist, P. A.; Pierloot, K.; Shahi, A. R. M.; Cramer, C. J.; Gagliardi, L. *J. Chem. Phys.* **2008**, *128*, 204109.
(13) Yanai, T.; Kurashige, Y.; Neuscamman, E.; Chan, G. K.-L. *J. Chem. Phys.* **2010**, *132*, 024105.
(14) Vaska, L. *Acc. Chem. Res.* **1976**, *9*, 175.
(15) Cramer, C. J.; Tolman, W. B. *Acc. Chem. Res.* **2007**, *40*, 601.
(16) Holland, P. L. *Dalton Trans.* **2010**, *39*, 5415.
(17) Cho, J.; Sarangi, R.; Annaraj, J.; Kim, S. Y.; Kubo, M.; Ogura, T.; Solomon, E. I.; Nam, W. *Nat. Chem.* **2009**, *1*, 568.
(18) Cho, J.; Sarangi, R.; Nam, W. *Acc. Chem. Res.* **2012**, *45*, 1321.
(19) Cramer, C. J.; Tolman, W. B.; Theopold, K. H.; Rheingold, A. L. *Proc. Natl. Acad. Sci. U.S.A.* **2003**, *100*, 3635.
(20) Suzuki, M. *Acc. Chem. Res.* **2007**, *40*, 609.
(21) Sarangi, R.; Cho, J.; Nam, W.; Solomon, E. I. *Inorg. Chem.* **2011**, *50*, 614.
(22) Cho, J.; Kang, H. Y.; Liu, L. V.; Sarangi, R.; Solomon, E. I.; Nam, W. *Chem. Sci.* **2013**, *4*, 1502.
(23) Zapata-Rivera, J.; Caballol, R.; Calzado, C. J. *J. Comput. Chem.* **2012**, *33*, 1407.
(24) Lewis, E. A.; Tolman, W. B. *Chem. Rev.* **2004**, *104*, 1047.
(25) Leclere, V.; Boiron, P.; Blondeau, R. *Curr. Microbiol.* **1999**, *39*, 365.
(26) Youn, H.-D.; Kim, E.-J.; Roe, J.-H.; Han, Y. C.; Kang, S.-O. *Biochem. J.* **1996**, *318*, 889.
(27) Youn, H.-D.; Youn, H.; Lee, J.-W.; Yim, Y.-I.; Lee, J. K.; Hah, Y. C.; Kang, S.-O. *Arch. Biochem. Biophys.* **1996**, *334*, 341.
(28) Wilke, G.; Schott, H.; Heimbach, P. *Angew. Chem., Int. Ed.* **1967**, *6*, 92.
(29) Lanci, M. P.; Brinkley, D. W.; Stone, K. L.; Smirnov, V. V.; Roth, J. P. *Angew. Chem., Int. Ed.* **2005**, *44*, 7273.
(30) Yao, S.; Bill, E.; Milsmann, C.; Wieghardt, K.; Driess, M. *Angew. Chem., Int. Ed.* **2008**, *47*, 7110.
(31) Aboelella, N. W.; Lewis, E. A.; Reynolds, A. M.; Brennessel, W. W.; Cramer, C. J.; Tolman, W. B. *J. Am. Chem. Soc.* **2002**, *124*, 10660.
(32) Aboelella, N. W.; Kryatov, S. V.; Gherman, B. F.; Brennessel, W. W.; Young, V. G.; Sarangi, R.; Rybak-Akimova, E. V.; Hodgson, K. O.; Hedman, B.; Solomon, E. I.; Cramer, C. J.; Tolman, W. B. *J. Am. Chem. Soc.* **2004**, *126*, 16896.
(33) Cramer, C. J.; Gour, J. R.; Kinal, A.; Wloch, M.; Piecuch, P.; Moughal Shahi, A. R.; Gagliardi, L. *J. Phys. Chem. A* **2008**, *112*, 3754.
(34) Gherman, B. F.; Cramer, C. J. *Inorg. Chem.* **2004**, *43*, 7281.
(35) Dickman, M. H.; Pope, M. T. *Chem. Rev.* **1994**, *94*, 569.
(36) Zapata-Rivera, J.; Caballol, R.; Calzado, C. J. *Phys. Chem. Chem. Phys.* **2011**, *13*, 20241.
(37) Zapata-Rivera, J.; Caballol, R.; Calzado, C. J. *J. Comput. Chem.* **2011**, *32*, 1144.
(38) Sarangi, R.; Aboelella, N.; Fujisawa, K.; Tolman, W. B.; Hedman, B.; Hodgson, K. O.; Solomon, E. I. *J. Am. Chem. Soc.* **2006**, *128*, 8286.
(39) Spencer, D. J. E.; Aboelella, N. W.; Reynolds, A. M.; Holland, P. L.; Tolman, W. B. *J. Am. Chem. Soc.* **2002**, *124*, 2108.
(40) Pantazis, D. A.; McGrady, J. E. *Inorg. Chem.* **2003**, *42*, 7734.
(41) Company, A.; Yao, S.; Ray, K.; Driess, M. *Chem.—Eur. J.* **2010**, *16*, 9669.
(42) Reynolds, A. M.; Lewis, E. A.; Aboelella, N. W.; Tolman, W. B. *Chem. Commun.* **2005**, *0*, 2014.
(43) Deng, Y.; Busch, D. H. *Inorg. Chem.* **1995**, *34*, 6380.
(44) Shan, X.; Que, L. *Proc. Natl. Acad. Sci. U.S.A.* **2005**, *102*, 5340.
(45) Maiti, D.; Lee, D.-H.; Gaoutchenova, K.; Würtele, C.; Holthausen, M. C.; Narducci Sarjeant, A. A.; Sundermeyer, J.; Schindler, S.; Karlin, K. D. *Angew. Chem., Int. Ed.* **2008**, *47*, 82.
(46) Maiti, D.; Fry, H. C.; Woertink, J. S.; Vance, M. A.; Solomon, E. I.; Karlin, K. D. *J. Am. Chem. Soc.* **2006**, *129*, 264.
(47) Finley, J.; Malmqvist, P.-Å.; Roos, B. O.; Serrano-Andrés, L. *Chem. Phys. Lett.* **1998**, *288*, 299.
(48) Halcrow, M. A. *Chem. Soc. Rev.* **2013**, *42*, 1784.
(49) Bersuker, I. B. *Chem. Rev.* **2001**, *101*, 1067.
(50) Bersuker, I. B. *Chem. Rev.* **2013**, *113*, 1351.
(51) Tao, J.; Perdew, J. P.; Staroverov, V. N.; Scuseria, G. E. *Phys. Rev. Lett.* **2003**, *91*, 146401.
(52) Andersson, K.; Roos, B. O. *Chem. Phys. Lett.* **1992**, *191*, 507.
(53) Merchán, M.; Pou-Amérigo, R.; Roos, B. O. *Chem. Phys. Lett.* **1996**, *252*, 405.
(54) Dolg, M.; Wedig, U.; Stoll, H.; Preuss, H. *J. Chem. Phys.* **1987**, *86*, 866.
(55) Frisch, M. J. *Gaussian 09, Revision B.01*; Gaussian, Inc.: Wallingford, CT, 2010.
(56) Aquilante, F.; De Vico, L.; Ferré, N.; Ghigo, G.; Malmqvist, P.-å.; Neogrády, P.; Pedersen, T. B.; Pitoňák, M.; Reiher, M.; Roos, B. O.; Serrano-Andrés, L.; Urban, M.; Veryazov, V.; Lindh, R. *J. Comput. Chem.* **2010**, *31*, 224.
(57) Veryazov, V.; Widmark, P.-O.; Serrano-Andrés, L.; Lindh, R.; Roos, B. O. *Int. J. Quantum Chem.* **2004**, *100*, 626.
(58) Karlström, G.; Lindh, R.; Malmqvist, P.-Å.; Roos, B. O.; Ryde, U.; Veryazov, V.; Widmark, P.-O.; Cossi, M.; Schimmelpfennig, B.; Neogrady, P.; Seijo, L. *Comput. Mater. Sci.* **2003**, *28*, 222.
(59) Aguilera-Iparraguirre, J.; Curran, H. J.; Klopper, W.; Simmie, J. M. *J. Phys. Chem. A* **2008**, *112*, 7047.
(60) Chen, H.; Lai, W.; Shaik, S. *J. Phys. Chem. Lett.* **2010**, *1*, 1533.
(61) Holland, P. L.; Cundari, T. R.; Perez, L. L.; Eckert, N. A.; Lachicotte, R. J. *J. Am. Chem. Soc.* **2002**, *124*, 14416.
(62) Panda, A.; Stender, M.; Wright, R. J.; Olmstead, M. M.; Klavins, P.; Power, P. P. *Inorg. Chem.* **2002**, *41*, 3909.
(63) For both $(N^{\wedge}N)_mCu(O_2)$ and $(N^{\wedge}N)_mCo(O_2)$, we could not find a stable C_S symmetrical structure unlike $(N^{\wedge}N)_mNi(O_2)$.
(64) For $(N^{\wedge}N)_mNi(O_2)$, $(N^{\wedge}N)_mCo(O_2)$, and $(Me_3P)_2Ni(O_2)$, 2-state-average (SA)-RASSCF calculation was performed. For $(N^{\wedge}N)_mCu(O_2)$, 3-SA-RASSCF was employed in order to ensure all the relevant orbitals in the active space. This is because some relevant orbitals move from the active space, in the case of 2-SA-RASSCF calculation.
(65) (a) The lone pair orbitals of $\hat{N}N$ and PMe_3 interact with the d_{yz} orbital in an anti-bonding way but does not with the d_{xy} orbital. Hence, the d_{yz} orbital is at higher energy than the d_{xy} orbital.[63c] (b) The overlap between the d_{yz} orbital and the π_z^* orbital of O_2 is much larger than the orbital overlap between the d_{xy} orbital and the π_x^* orbital of O_2, because the former is the π-type overlap but the latter is the δ-type one. Hence, the splitting between the bonding and anti-bonding orbitals is much larger in the d_{xz} orbital than in the d_{xy} orbital. (c) Albright, T. A.; Hoffmann, R.; Thibeault, J. C.; Thorn, D. L. *J. Am. Chem. Soc.* **1979**, *101*, 3801.
(66) The active space for $(Me_3P)_2Ni(O_2)$ includes five 3d orbital, five 4d orbitals, and two π^* orbitals of O_2 moiety; in total, 12 electrons in 12 orbitals.
(67) Baba, H.; Suzuki, S.; Takemura, T. *J. Chem. Phys.* **1969**, *50*, 2078.
(68) Fujimoto, H.; Kato, S.; Yamabe, S.; Fukui, K. *J. Chem. Phys.* **1974**, *60*, 572.
(69) Dapprich, S.; Frenking, G. *J. Phys. Chem.* **1995**, *99*, 9352.
(70) Takagi, N.; Sakaki, S. *J. Am. Chem. Soc.* **2012**, *134*, 11749.
(71) Zeng, G.; Sakaki, S. *Inorg. Chem.* **2012**, *51*, 4597.
(72) Ochi, N.; Nakao, Y.; Sato, H.; Matano, Y.; Imahori, H.; Sakaki, S. *J. Am. Chem. Soc.* **2009**, *131*, 10955.
(73) Zeng, G.; Sakaki, S. *Inorg. Chem.* **2011**, *50*, 5290.
(74) Ghosh, D.; Biswas, R. *Int. J. Mol. Sci* **2003**, *4*, 379.
(75) The radius of Ni^+ is computed by the comparison the Ni—O distances in the C_4 symmetrical square planar $[Ni^I(H_2O)_4]^+$ and $[Ni^{II}(H_2O)_4]^{2+}$ optimized by TPSSTPSS functional with the same basis sets to $(N^{\wedge}N)Ni(O_2)$. The radius of Ni^+ is equal to the sum of the difference of the Ni—O distance in these model complexes and the radius of Ni^{2+} in ref 68.
(76) Ishikawa, A.; Tanimura, Y.; Nakao, Y.; Sato, H.; Sakaki, S. *Organometallics* **2012**, *31*, 8189.
(77) de Visser, S. P.; Rohde, J.-U.; Lee, Y.-M.; Cho, J.; Nam, W. *Coord. Chem. Rev.* **2013**, *257*, 381.

(78) Latifi, R.; Tahsini, L.; Kumar, D.; Sastry, G. N.; Nam, W.; de Visser, S. P. *Chem. Commun.* **2011**, *47*, 10674.
(79) Liu, L. V.; Hong, S.; Cho, J.; Nam, W.; Solomon, E. I. *J. Am. Chem. Soc.* **2013**, *135*, 3286.
(80) Cho, J.; Woo, J.; Eun Han, J.; Kubo, M.; Ogura, T.; Nam, W. *Chem. Sci.* **2011**, *2*, 2057.
(81) Cho, J.; Sarangi, R.; Kang, H. Y.; Lee, J. Y.; Kubo, M.; Ogura, T.; Solomon, E. I.; Nam, W. *J. Am. Chem. Soc.* **2010**, *132*, 16977.
(82) Sastri, C. V.; Lee, J.; Oh, K.; Lee, Y. J.; Lee, J.; Jackson, T. A.; Ray, K.; Hirao, H.; Shin, W.; Halfen, J. A.; Kim, J.; Que, L.; Shaik, S.; Nam, W. *Proc. Natl. Acad. Sci. U.S.A.* **2007**, *104*, 19181.
(83) Fiedler, A. T.; Que, L. *Inorg. Chem.* **2009**, *48*, 11038.